

The ECPC Coupled Prediction Model

E. YULAEVA, M. KANAMITSU, AND J. ROADS

Experimental Climate Prediction Center, Climate Research Division, Scripps Institution of Oceanography, University of California, San Diego, La Jolla, California

(Manuscript received 29 June 2006, in final form 20 February 2007)

ABSTRACT

This paper presents a new Experimental Climate Prediction Center (ECPC) Coupled Prediction Model (ECPM). The ECPM includes the Jet Propulsion Laboratory (JPL) version of the Massachusetts Institute of Technology (MIT) ocean model coupled to the ECPC version of the National Centers for Environmental Prediction (NCEP) Atmospheric Global Spectral Model (GSM). The adjoint and forward versions of the MIT model forced with the NCEP atmospheric analyses are routinely used at JPL for ocean state assimilation. An earlier version of the GSM was used for the NCEP–Department of Energy reanalysis-2 project and for operational seasonal forecasts at NCEP. The ECPM climatology and internal variability derived from a 56-yr-long coupled integration are compared with the observations and reanalysis data. Though the ECPM exhibits climatological biases, these biases are relatively small and comparable to the systematic errors produced by other well-known coupled models, including the recent NCEP Climate Forecast System. The internal variability of the model resembles the observations. ECPM simulates both seasonal and interannual variability in the tropical Pacific reasonably well. The model has good skill in reproducing the mechanism of ENSO evolution as well as ENSO teleconnection patterns (including the Indian monsoon–ENSO relationship). The skill of the ECPM in predicting 1994–2006 SST anomalies over the Niño-3.4 region is shown to be comparable to other coupled models. These retrospective forecasts were used for deriving a model climatology for real-time seasonal forecasts that are currently produced and displayed at ECPC.

1. Introduction

Dynamical seasonal forecasts with time scales ranging from a few months to a year are now commonly performed at operational weather centers around the world. Although the accuracy of the forecasts are still marginal in comparison to statistical methods (Oldenborgh et al. 2005; Saha et al. 2006) continued efforts to improve the numerical modeling systems should eventually provide dynamical seasonal forecast products as useful as current dynamical forecasts for short- and medium-range predictions. In addition, unlike statistical methods, a dynamical forecast model is capable of providing other valuable data that can be used to understand the evolution of the atmosphere and ocean, and can thus further improve future seasonal prediction itself.

There are currently two kinds of dynamical seasonal forecasting methodologies. One forces an atmospheric model with independently predicted sea surface temperature anomalies (SSTAs). Predicted SSTAs are produced either by purely statistical methods (i.e., persisted anomalies) or by combined statistical and ocean–atmosphere coupled system forecasts. This method is called a “two-tier” forecast, and is used widely because it is easier to implement and simpler to make a reasonable forecast (see, e.g., Roads et al. 2001; Kanamitsu et al. 2002a; Straus et al. 2003). The weakness of this method is that the atmospheric model is forced by the SST but the ocean is not subsequently affected by the atmosphere. In the real world, the SST is determined by the mutual interaction between the ocean and atmosphere, and the two-tier models’ lack of interaction may result in unphysical behaviors. For example, in regions where SST anomalies are driven by the atmosphere (like the central North Pacific and tropical monsoon regions) there could be huge discrepancies between simulated and observed direction of the air–sea flux exchange in the two-tier system. As was shown in Wu et

Corresponding author address: Dr. Elena Yulaeva, Experimental Climate Prediction Center, Climate Research Division, Scripps Institution of Oceanography, University of California, San Diego, 0224, La Jolla, CA 92093-0224.
E-mail: eyulaeva@ucsd.edu

al. (2006), the inclusion of coupling increases the skill of the simulation of the air–sea interaction, which then leads to a better prediction of monsoon activity

The second method is to use a dynamically coupled ocean–atmosphere system, the “one-tier” forecast. Initially a statistical or empirical correction (flux adjustment) was frequently used at the interface between the ocean and atmospheric models but recent improvements in both atmospheric and ocean models have now made it possible to avoid such corrections. Some form of statistical correction may still be needed for the final model output, but the forecast system itself is free from statistical corrections and thus the state of the ocean, including SST, and the atmosphere are dynamically and physically consistent and not overly artificially constrained.

The factors that greatly influence the skill of the seasonal forecast (in addition to the accuracy of the atmospheric and ocean models, and their coupling method) are the initial conditions. For an atmospheric forecast, the initial conditions are not crucial for time leads beyond about a month, because long-term forecasts are boundary-forcing problems (e.g., Reichler and Roads 2003). However, certain atmospheric initial conditions, including those associated with anomalous stratosphere states, may still be important (Baldwin and Dunkerton 1999; Reichler and Roads 2004, 2005a,b). Oceanic initial conditions are certainly critical, because the seasonal ocean forecast is an initial value problem. In fact, in some cases ocean forecasts out to at least a year are strongly dependent on how accurate the ocean initial conditions were. In addition, the ocean initial conditions need to be “balanced” with the ocean and atmospheric models, otherwise, the integration goes through an initial adjustment, which contaminates the initial ocean condition and makes it difficult to use the forecast during the adjustment period. This adjustment period frequently exceeds several months, nearly the entire duration of the seasonal forecast (e.g., Rosati et al. 1997). In this regard, a data assimilation system for the ocean is critical for a coupled model seasonal forecast; just like atmospheric data assimilation is essential for short- and medium-range atmospheric forecasts. There are additional requirements for land and ocean sea ice initial conditions, but we will not delve into this further because our focus here is on ocean–atmosphere interactions.

When we actually perform a real-time coupled forecast, the requirement of accurate ocean initial conditions places severe limits on the choice of ocean model, because the ocean model needs to have its own data assimilation, and in addition the ocean analysis system needs to be running in near–real time. Variational data

assimilation usually involves developing an adjoint of the ocean model, which requires considerable expertise and time to develop. The most widely used ocean model with a data assimilation component is the Geophysical Fluid Dynamics Laboratory (GFDL) Modular Ocean Model (MOM; see Derber and Rosati 1989; Carton et al. 2000). This ocean data assimilation has now been running in real time at the National Centers for Environmental Prediction (NCEP; Ji et al. 1995; Ji et al. 1998) for more than 10 yr. MOM is very portable and easy to adopt, thus, most coupled models developed and used in the United States utilize the GFDL ocean model, with a wide variety of atmospheric models coupled to it. Unfortunately, this current limited ocean analysis and model choice may severely limit the true scope of multimodel ensemble coupled model forecasts. At least the coupled forecast system at the National Aeronautics and Space Administration (NASA) Global Modeling and Assimilation Office (GMAO), developed by Schopf and Loughe (1995), does provide an independent ocean model and analysis.

In this paper, we present a new seasonal forecast system, which utilizes an ocean model developed independently from GFDL and NASA GMAO, coupled to our version of the NCEP seasonal forecast model. The oceanic component of this forecast system is the Massachusetts Institute of Technology (MIT) model that comes with an advanced 4D variational data assimilation system. Though the MIT GCM was primarily developed for research, ocean assimilation has been run quasi operationally at the Jet Propulsion Laboratory (JPL) for the last several years. Cazes-Boezio et al. (2008) used JPL’s version of the MIT OGCM coupled to the University of California, Los Angeles (UCLA) atmospheric GCM (AGCM) to confirm that initialization of the coupled model with the physically consistent JPL ocean state assimilated data significantly improves the skill of the seasonal climate forecasts. We will demonstrate that our new one-tier Experimental Climate Prediction Center (ECPC; information online at <http://ecpc.ucsd.edu/>) Coupled Prediction Model (ECPM), without flux adjustment, produces skillful seasonal forecasts, which are comparable to other coupled forecast systems.

One rather important component of the seasonal forecast, missing in this study, needs to be mentioned here. A seasonal forecast is itself probabilistic in nature, particularly the atmospheric part, but also the coupled ocean component. The natural variability that is essentially noise in the forecast has to be filtered out by computing ensemble averages. A probability density function can also be obtained from ensemble forecasting, although its usage is still limited. Unfortunately, we

did not have sufficient computer resources to perform large ensemble predictions in this initial study. All of the forecasts presented here consist of a single-member deterministic forecast. Therefore, we concentrate here on the average error components of the atmosphere and ocean on broad scales (e.g., Moore and Kleeman 1996).

This paper is structured as follows. After first describing the coupled modeling system in section 2, we will describe the main mean features of a long, continuous coupled model integration starting with consistent oceanic and atmospheric conditions in section 3. We then examine internal variability of the model in section 4. Section 5 presents many coupled model retrospective forecasts starting at different months and examines how the skill of the seasonal forecast depends on the initial conditions and forecast lead time. Section 6 concludes the paper.

2. Models and experiments

ECPM consists of the ECPC version of the NCEP Global Spectral Model (GSM) and the JPL version of the MIT ocean model that has been used for ocean analysis each month beginning in 1993. The coupling is performed every 24 h. The atmospheric model net heat, freshwater, and short- and longwave radiation fluxes, together with wind stresses, are passed to the ocean component, while the atmosphere is forced with the SSTs obtained from the oceanic module. No flux adjustment is used in the coupled system. A difference between the ECPC coupling procedure and the one utilized in the NCEP Climate Forecast System (CFS) is that the numerical interaction between the atmosphere and ocean is global, and not confined to climatology at higher latitudes. The only climatology that is currently used in the model is the sea ice extent. We are planning to eventually include the correct description of the internal ice dynamics that will then allow for more realistic heat and freshwater transports and better calculation of air–sea fluxes at high latitudes. Further details about the models are provided below.

a. MIT OGCM

The oceanic component of the ECPM is the JPL MIT model, which has $1^\circ \times 1^\circ$ horizontal resolution with a telescoping ($1/3^\circ$) resolution near the equator. The ocean model also has fine vertical resolution with 46 vertical levels. The vertical depth goes down to 5800 m, with the first 23 levels located in the upper 400 m. The model is based on the primitive equations on a sphere under the Boussinesq approximation. There are prognostic equations for horizontal velocity, heat, and salt, which are integrated forward in time on a staggered

grid. At each time step the internal pressure is calculated from the hydrostatic relation, and the vertical velocity is diagnosed from the continuity equation. Spatial coordinates are longitude, latitude, and height. A detailed description of the model is provided in Marshall et al. (1997a,b). We are using the version of the model with an implicit free surface. A full surface nonlocal *K*-profile parameterization (KPP) of vertical mixing throughout a water column is also used, and is described in detail in Large et al. (1994). The KPP model of vertical mixing parameterization is based on parameters derived from observational data; thus, it captures important physics during the annual cycle for a wide range of dynamical regimes and at the same time does not significantly increase computational time. A convective adjustment is used to remove gravitational instabilities underneath the surface mixed layer.

Finite-volume techniques are employed yielding an intuitive discretization and support for the treatment of irregular geometries with orthogonal curvilinear grids. The algorithm can conveniently exploit massively parallel computers and has a domain decomposition, which allocates vertical columns of ocean to each processing unit. The model can arbitrarily handle complex geometry and is efficient and scalable. A “pressure correction” method is used, which is solved as a Poisson equation for the pressure field with Neumann boundary conditions in a geometry as complicated as that of the ocean basins. The pressure field is separated into surface, hydrostatic, and nonhydrostatic components. A preconditioned conjugate-gradient iteration is used to invert symmetric elliptic operators in both two and three dimensions. Physically motivated preconditioners are designed, which are efficient at reducing computation and minimizing communication between processors.

The assimilation (Kalman filter with Green’s function tuned parameters) and forward simulation versions of the MIT model forced with NCEP reanalysis data are routinely used at JPL for ocean state assimilation (Fukumori 2002). To produce a computationally efficient data assimilation, JPL adopted a hierarchical assimilation system. First, a series of Green’s function are calculated and used for the correction of robust biases in the mean state; second, a Kalman filter and smoother produces near-real-time analysis of the time-dependent state. The system assimilates observed sea level and temperature profiles. (Near-real-time analyses are available at the JPL data server online at <http://ecco.jpl.nasa.gov/external> as 10-day averages.)

The ocean analysis has been used in numerous studies of ocean variability as well as in various geodetic studies. These studies have demonstrated the accuracy

of the JPL data assimilation system (e.g., Dickey et al. 2002; Stammer et al. 2002) and its applicability for a wide range of climate variability studies.

b. GSM

The atmospheric component of the ECPM is the ECPC version of the NCEP GSM (Kanamitsu et al. 2003). An earlier version of the GSM is being used for operational seasonal forecasting at NCEP and its performance was documented in Kanamitsu et al. (2003). (An upgraded version of the model is used as the atmospheric component in the current NCEP CFS.) Two-tier ensemble forecasts of the ECPC GSM are routinely being provided to the International Research Institute for Climate and Society (IRI) as part of their multimodel seasonal forecast ensemble. Robertson et al. (2004) showed that the addition of these two-tier ECPC forecasts increased the IRI multimodel forecast skill, especially over Africa.

The GSM utilizes spherical harmonics as the basis functions and has an efficient transformation to a Gaussian grid for calculation of nonlinear terms and physics. Horizontal resolution is T62 (~200 km), but the number of grid points is reduced in higher latitudes to save computer time (Juang 2004). There are 28 vertical sigma (Phillips 1959) coordinate levels. The vertical domain is from the earth's surface ($\sigma = 1$) to the top of the atmosphere ($\sigma = 0$). This domain is divided into 28 layers with enhanced resolution near the bottom and the top of the model. Global and regional versions of the model are also used for experimental subseasonal-to-seasonal climate predictions at ECPC (see Roads 2004). The main time integration scheme is the leapfrog scheme for nonlinear advection terms, and the semi-implicit scheme for gravity waves. An Asselin (1972) time filter is used to reduce computational modes.

Atmospheric model dynamics are based on the conservation of mass, momentum, energy, and moisture. To take advantage of the spectral technique in the horizontal, the momentum equation is replaced by the vorticity and divergence equations (Bourke 1974). Thus, the model is basically described as a set of primitive equations with vorticity, divergence, logarithm of surface pressure, specific humidity, and virtual temperature as dependent variables. Scale-selective, second-order horizontal diffusion (Leith 1971) is applied to vorticity, divergence, and virtual temperature. The diffusion of temperature is performed on quasi-constant pressure surfaces (Kanamitsu et al. 1991). Implicit integration with a special time filter (Kalnay and Kanamitsu 1988) is used for vertical diffusion. To incorporate physical tendencies into the semi-implicit integra-

tion scheme, a special adjustment scheme is performed (Kanamitsu et al. 1991).

The physics are written in the form of an adjustment and executed in sequence. The physical processes parameterizations originated from the NCEP–Department of Energy (DOE) reanalysis-2 (R-2; see Kanamitsu et al. 2002a,b). These parameterizations include long- and shortwave radiation (Chou and Suarez 1994; Chou and Lee 1996) interacting with clouds, which are diagnosed from relative humidity, convective activity (Slingo 1987), relaxed Arakawa–Schubert convection scheme (Moorthi and Suarez 1992), turbulent mixing and heat and moisture exchanges at the earth's interfaces based on the Monin–Obukhof similarity theory, nonlocal vertical diffusion scheme in the planetary boundary layer (Hong and Pan 1996), the Oregon State University land model (Pan and Mahrt 1987), shallow convection (Tiedtke 1983), gravity wave drag (Alpert et al. 1988), and use of smoothed mean orography.

3. Model climatology

As was noted above, the ability of the coupled model to reproduce climatology and internal variability is a prerequisite for producing skillful forecasts. An investigation of the deviation between model and observed climatology might be used as one of the strategies for making subsequent improvements. In this section we document the ECPM climatology and deviation from observations, and show that the biases are small and the internal variability is realistic. No artificial flux coupling has therefore been needed.

a. Atmospheric temperature and winds

Figure 1 shows height–latitude cross sections of the zonal mean December–February (DJF; top-left panel) and June–August (JJA; top-right panel) temperature profiles obtained from the 56 yr of ECPM integration and the corresponding model's biases expressed as the difference between the coupled model climatology and the 56-yr (1950–2005) R-2 climatology. During the wintertime (bottom-left panel), the ECPM produces a cold bias in the Northern Hemisphere. The warm bias in high latitudes, especially in the Southern Hemisphere, accompanies this cold bias. The cold bias in the troposphere has a pronounced maximum at around 700 hPa and might be caused by a deficiency in cloud and convection parameterizations. The model's lower stratosphere is colder by around 5 K. These biases are similar to the ones produced by the stand-alone atmospheric model in the Atmospheric Model Intercomparison Project (AMIP)-type integration (e.g., Martin et al. 2006); therefore, they should be explained by the atmospheric behavior, and not by the coupled processes. The

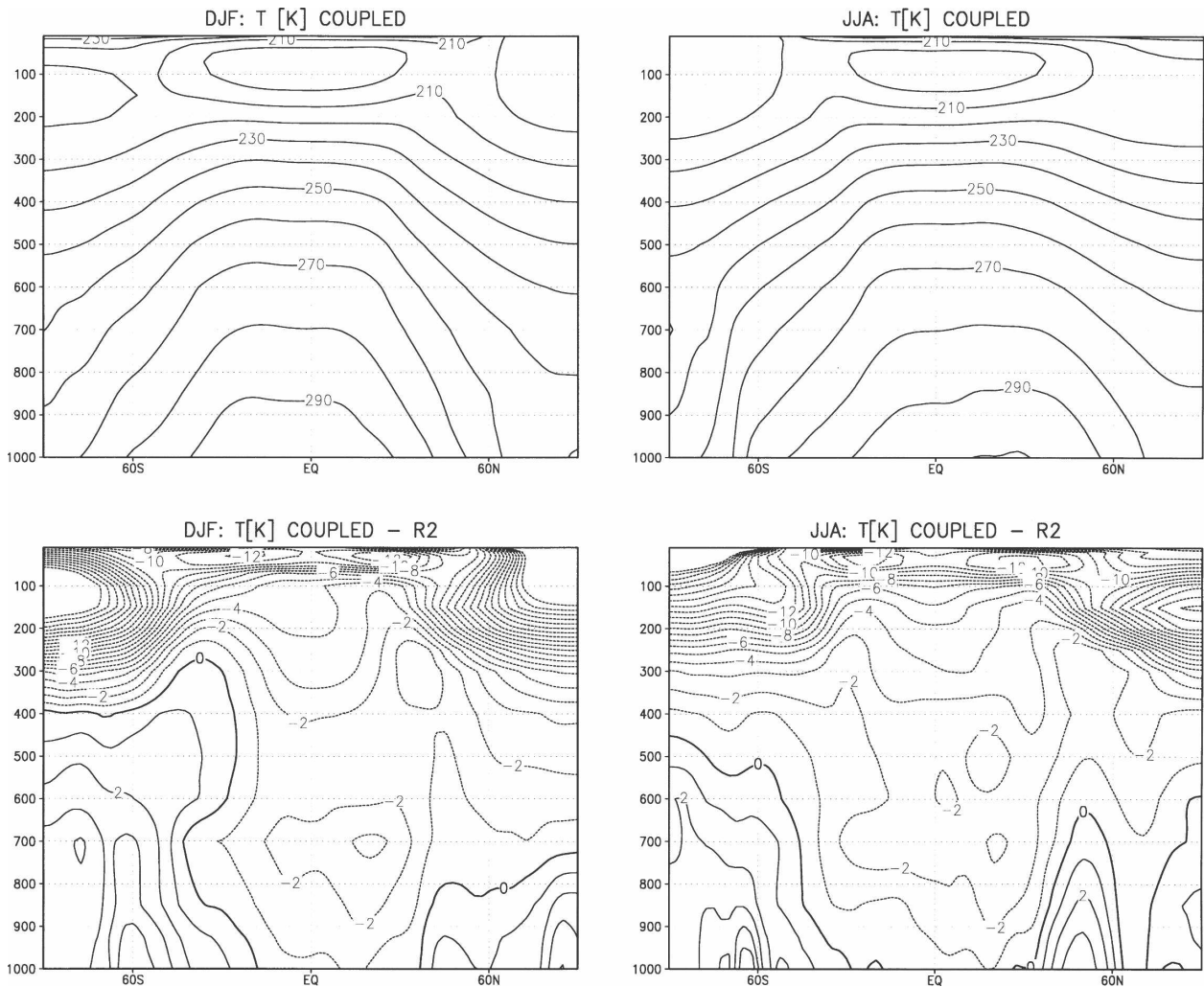


FIG. 1. Height–latitude cross sections during the boreal (left) winter and (right) summer of the zonal mean temperature profiles obtained from a long integration of (top) the ECPM. (bottom) The differences between the coupled model simulation and the corresponding R-2 data. The contour interval is 10 K for the full fields and 1 K for the differences. The boldface contour in the difference maps shows the zero values.

difference in the temperature distribution during boreal summer, JJA, is shown in the bottom-right panel and is qualitatively the same. The warmer near-surface bias shifts toward the equator in the Northern Hemisphere, and the tropical midtroposphere cold biases are less pronounced.

The temperature biases exhibited in the middle and upper troposphere are somewhat similar to the corresponding biases exhibited by the two versions of the GFDL Global Coupled Model, GFDL CM2.0 and GFDL CM2.1 (Delworth et al. 2006). However, the GFDL CM2.0 and GFDL CM2.1 exhibit pronounced warm biases in the equatorial and tropical parts of the lower troposphere. The ECPM produces colder-than-observed temperatures in the whole bulk of the tropical troposphere. Overall, the magnitude of the atmospheric

temperature errors is larger than the atmospheric model run forced by observed SST (Kanamitsu et al. 2002a), reflecting the systematic error in the simulation of SST.

Figure 2 exhibits the systematic error in the simulation of the climatological SST. In comparison to the NCEP optimum interpolation (OI) SST averaged from 1950 to 2005, the ECPM produced an SST 0.5–1 K colder over most of the Tropics. On the other hand, the ECPM produces a warmer SST over the northern oceans, especially over the western and central North Pacific during the summertime. The central Pacific equatorial cold bias is also produced by a number of coupled models including the University of California, Los Angeles global atmospheric model coupled to the GFDL oceanic model (Robertson et al. 1995), the

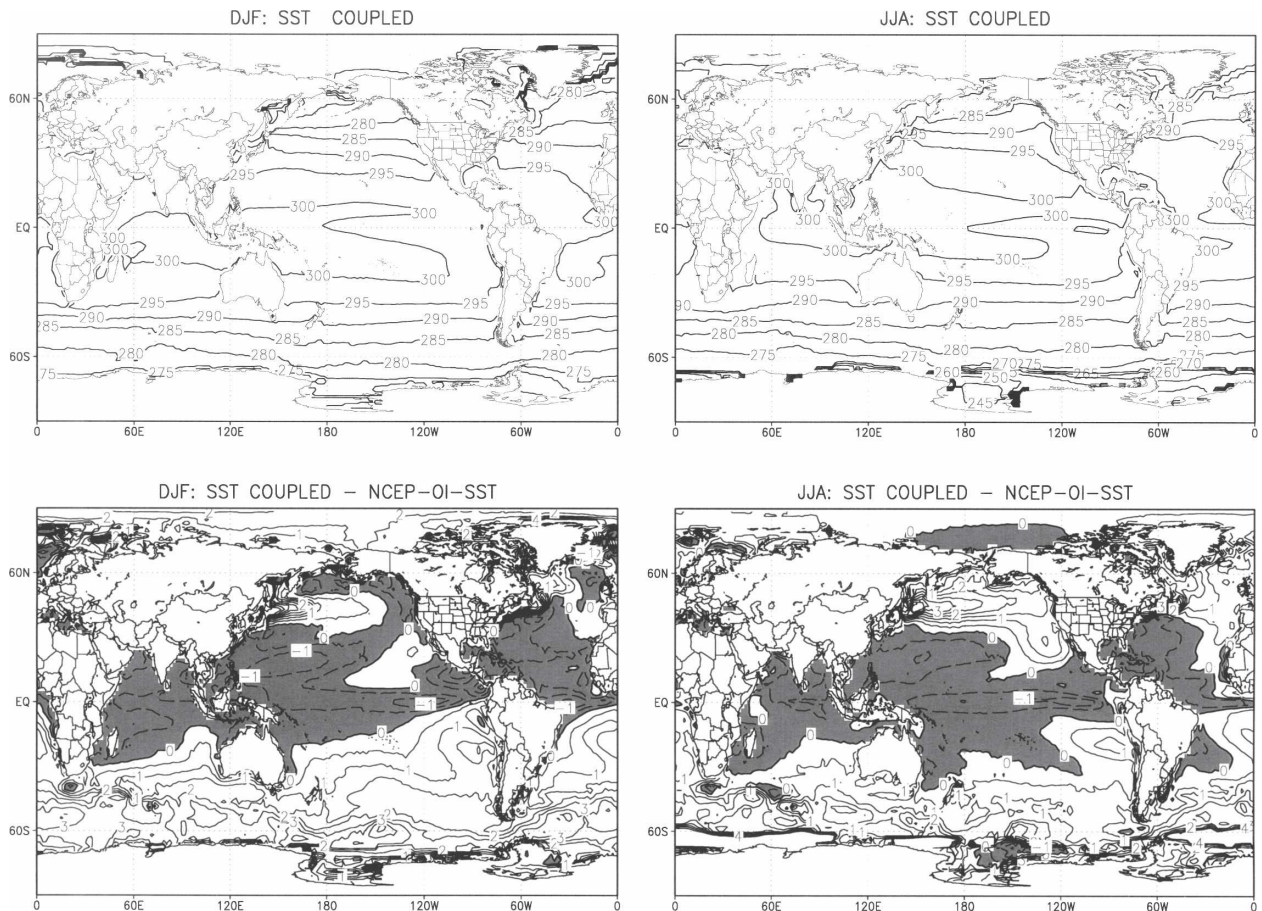


FIG. 2. Boreal (left) winter and (right) summer SST obtained from a long integration of (top) the ECPM. (bottom) The difference between ECPM simulation and corresponding NCEP OI SST data. The contour interval is 5 K for the full fields and 0.5 K for the differences. Negative values are shaded.

GFDL CM2.0 and CM2.1 (Delworth et al. 2006), the Florida State University (FSU) climate model (Shin et al. 2005), and the Hadley Centre Global Environmental Model version 1 (HadGEM1; Johns et al. 2006).

The systematic errors in the precipitation field are shown in Fig. 3. The Climate Prediction Center (CPC) Merged Analysis of Precipitation (CMAP) for 1979–2004 was used for the observational data. The differences between the ECPM and CMAP are shown in the second row from the top. The corresponding differences between R-2 (1950–2005) and CMAP precipitation are shown in the bottom row. The ECPM wintertime intertropical convergence zone (ITCZ), shown in the top left panel in Fig. 3, reveals two zonal bands of maximum precipitation (the so-called double-ITCZ feature) mainly in the tropical western Pacific. ECPM extends the wintertime double-ITCZ feature into the central Pacific as marked by excessive precipitation around 5°N in the central tropical Pacific (second down from the top-left panel in Fig. 3). However, as opposed

to a number of coupled model climatologies, the double-ITCZ feature is not extended all the way into the eastern Pacific. During the summertime (right column in Fig. 3), the model underestimates the western equatorial Pacific precipitation (second down from the top-right panel), and thus separates the nearly uniform band of maximum precipitation, thus creating the double-ITCZ feature in the western Pacific. Comparison with the precipitation from R-2 (third row from the top) indicates that the coupled model produces more realistic wintertime climatology over the northern oceans than the R-2. This is especially evident over the Kuroshio–Oyashio Extension (KOE) region (second down from the top-left and bottom-left panels), where the R-2 DJF precipitation pattern reveals an excessive amount of precipitation. This bias is reduced in the coupled model. It should be noted that the double-ITCZ feature is present in almost all of the current coupled models (e.g., Delworth et al. 2006; Johns et al. 2006). As was noted in Johns et al. (2006), this phe-

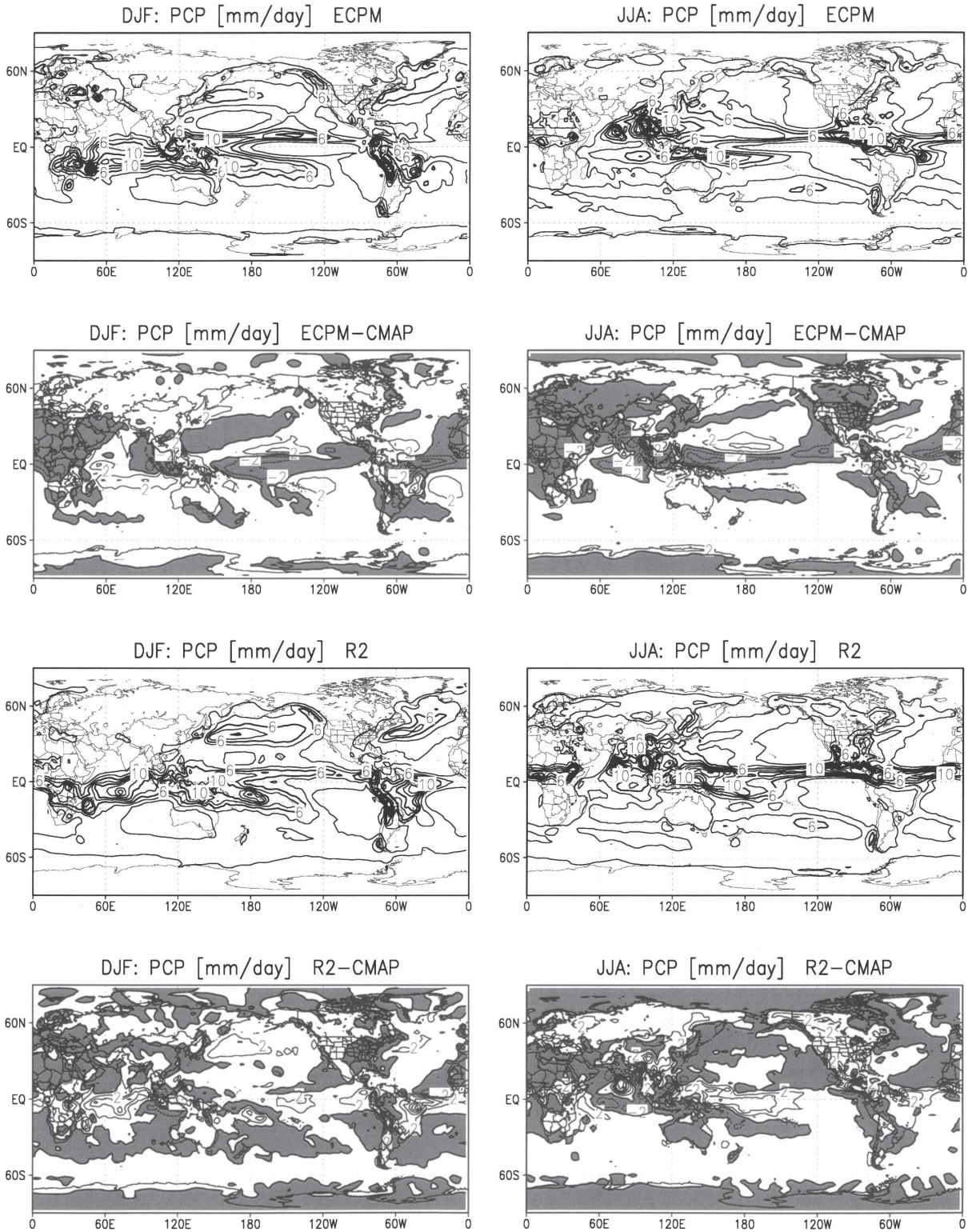


FIG. 3. (left) DJF and (right) JJA precipitation obtained from (top) 56-yr-long ECPM integration. Difference between (second from top) ECPM and CMAP climatology and (third from top) R-2 precipitation climatology. (bottom) Difference between R-2 and CMAP climatology. The contour interval is 1 mm day⁻¹. Negative values are shaded.

nomenon may be linked to the equatorial cold bias exhibited by many coupled models. The precipitation biases in the ECPM are comparable to the corresponding biases in the GFDL CM2.0 and CM2.1 (e.g., Fig. 17 in Delworth et al. 2006).

The corresponding ECPM zonally averaged zonal winds (not shown here) exhibit biases comparable with the corresponding biases both in the GFDL Global Atmosphere and Land Model (AM2-LM2) AMIP-type simulation (GFDL Global Atmospheric Model Development Team 2004) and in the GFDL CM2.0/CM2.1 coupled (Delworth et al. 2006) integrations. The largest discrepancies from the observations (around 10–15 m s^{-1}) occur in the lower stratosphere. These biases are associated with the cold biases in the zonal mean temperature in accordance with the thermal wind equation. In the troposphere, the differences are much smaller.

The error in the Northern Hemisphere zonal wind extends to the surface and is accompanied by a dipole pattern in the sea level pressure bias pattern that consists of an increased surface cyclonic activities in high latitudes, and increased anticyclonic activities in mid-latitudes.

The model produces a stationary planetary wave pattern (depicting departures from the zonal mean 500-mb geopotential height field during boreal winter, not shown here) that is similar to the ones obtained from R-2 and simulated by the GFDL CM2.0 and CM2.1 (i.e., Fig. 23 of Delworth et al. 2006). Similar to the GFDL CM2.0 and CM2.1, the ECPM produces weaker troughs over the North Pacific and northeastern parts of North America, and a weaker ridge over the west coast of the United States during boreal winter.

Summarizing, both winter- and summertime ECPM circulations exhibit systematic biases in comparison to R-2 and observations. However, these biases are comparable with the biases produced by other climate models (Anderson et al. 2004; Saha et al. 2006; Delworth et al. 2006).

b. Ocean climatology

One of the most important variables indicating the potential influence of the ocean on the atmosphere is the integrated heat content from the surface to 400-m depth (e.g., McPhaden 2004) because it can be considered to be a predictor of ENSO development. Therefore, the difference between the model and observed oceanic heat content climatology is an indicator of how good the ocean simulation is. Figure 4 exhibits the annual mean 400-m heat content obtained from the coupled integration (top panel). Difference between the JPL 1993–2005 assimilated data and the climatology

from the ECPM long run is shown in the bottom panel. The maximum absolute difference between the coupled model run and the assimilated data in the Tropics is less than $1.5 \times 10^9 \text{ J m}^{-2}$, which is around 10% of the seasonal mean value. The most pronounced differences are seen over the eastern part of the equatorial Pacific and at around 10°N in the western Pacific. This is a typical bias pattern for coupled model simulations, and is associated with the ITCZ location. ECPM exhibits a positive bias over the KOE region in the western North Pacific. Again, errors of the same size and sign are typical of other coupled models (e.g., Megann 2005). The possible causes of these errors will be discussed later in section 4c.

A depth–longitude temperature cross section along the equator is shown in Fig. 5. Again, as for the 400-m heat content, the top panel shows ECPM annual mean simulated data, and the bottom panel shows the difference between the JPL analysis and the climatology of the coupled model. The greatest difference can be seen in the western Pacific in the barrier layer below the thermocline. In the eastern Pacific, the model tends to produce a deeper thermocline. It should be mentioned that the absolute values of the discrepancies between the model and assimilated data are small in comparison to the climatology (less than 5% of the absolute values). These biases are qualitatively similar to the ones produced by the GFDL CM2.0 and CM2.1 (Wittenberg et al. 2006) and to the biases produced by Green's function estimate of ocean temperature data (Menemenlis et al. 2005).

To summarize, the ECPM climatology exhibits biases in comparison to observations. However, the amplitudes of these biases are much smaller than the mean values, and the discrepancies are comparable or smaller than the systematic errors produced by most coupled models used for climate prediction (e.g., Saha et al. 2006; Gordon et al. 2000).

4. Internal variability

In the previous section we documented the mean model state and the deviations from observations. Though correcting these systematic errors could perhaps be made by attempting to tune the model, a more important question is the extent to which the model can reproduce local observed variability as well as the remote atmospheric response of various variables. In that regard, the tropical El Niño–Southern Oscillation (ENSO) signal is the most important global signal observed in climate variables. We therefore first checked the ability of the model to produce realistic SST variability in the tropical region.

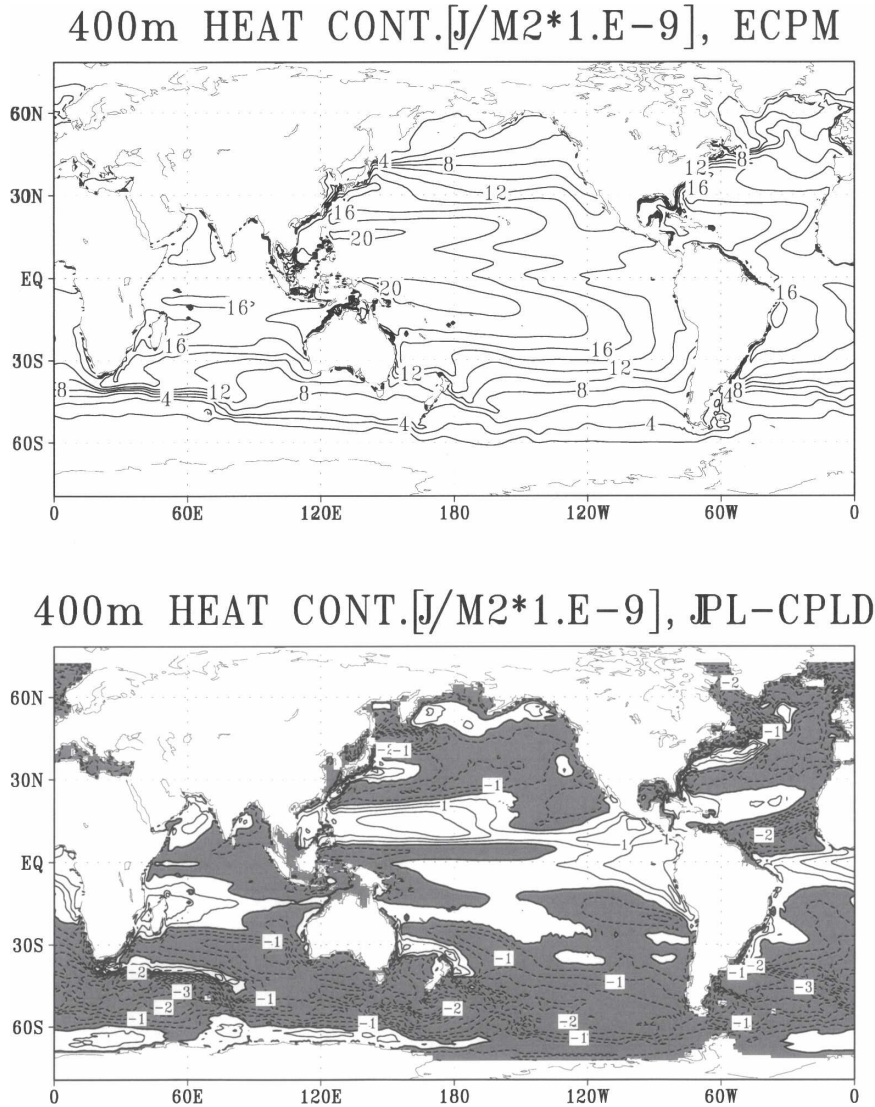


FIG. 4. (top) Annual mean 400-m heat content simulated by ECPM. (bottom) The difference between JPL MIT assimilated 1993–2005 data and the ECPM 56-yr integration. The contour interval 2 J m^{-2} for the full fields and 0.5 J m^{-2} for the differences. The boldface contour in the difference maps shows the zero values. Negative values are shaded.

a. Seasonal cycle in the tropical Pacific

Li and Philander (1996) demonstrated the importance of correct simulations of the annual cycle in the tropical Pacific and its connection to the mean state. Therefore, the ECPM’s ability to correctly simulate annual variability and phase locking will be studied in this section.

The model’s SST annual cycle (Fig. 6, bottom-left panel) exhibits a semiannual cycle in the western equatorial Pacific, and a westward-propagating annual signal in the eastern Pacific. This annual variability is very close to both the Hadley Centre Sea Ice and SST

dataset shown in Jungclaus et al. (2006) and the NCEP OI SSTs shown in Wittenberg et al. (2006). The ECPM outperforms the coupled model that consists of the Max Planck Institute for Meteorology (MPI-M), version 5, atmospheric model (ECHAM5) and the Max Planck Institute Ocean Model (MPI-OM) (ECHAM5/MPI-OM) in reproducing the phase and strength of the equatorial Pacific SSTs. However, similar to the GFDL CM2.0 and CM2.1, the ECPM produces a stronger-than-observed annual cycle (see Wittenberg et al. 2006, their Fig. 11a). The corresponding annual mean pattern (Fig. 6, top-left panel) is quantitatively in close agreement with observations. There are both a pronounced

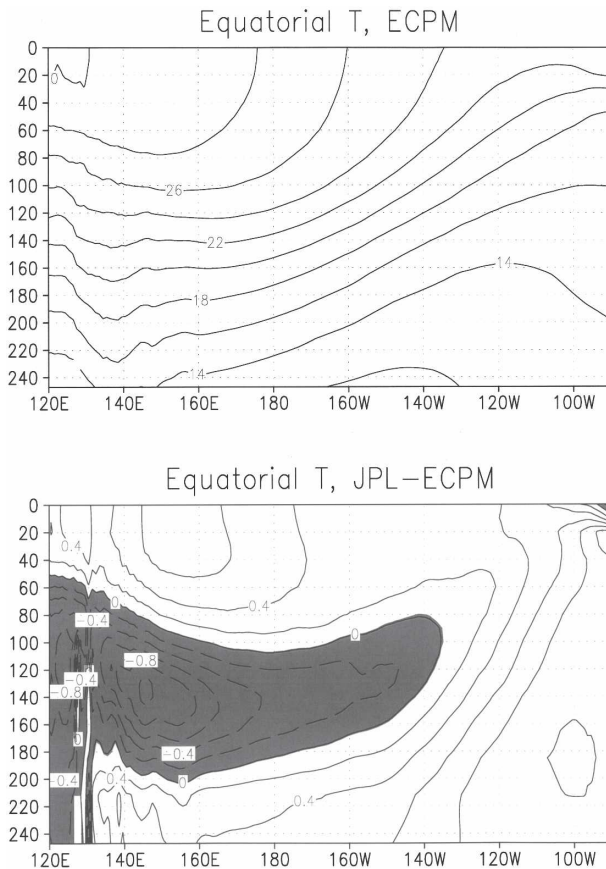


FIG. 5. (top) ECPM annual mean height-latitude cross section of the ocean temperature field averaged from 5°N to 5°S . (bottom) The difference between JPL MIT assimilated 1993–2005 data and the ECPM 56-yr integration. The contour interval is 2 K for the full field and 0.2 K for the differences. Negative values are shaded.

warm pool and a cold tongue, although the ECPM produces a cold bias over the cold tongue region.

The top-right panel in Fig. 6 shows the annual mean zonal wind stress. The wind stress pattern is similar to the 40-yr European Centre for Medium-Range Weather Forecasts (ECMWF) Re-Analysis (ERA-40) data (see Wittenberg et al. 2006). The annual mean pattern exhibits easterlies maxima at around 20°N and 150°W – 180° , and weak westerlies at the equatorial western and eastern boundaries. The bottom-right panel shows the annual cycle of the zonal wind stress averaged over 2°S – 2°N . The model captures the westward propagation of the east Pacific signal, as well as the observed relaxation of the trade winds during the spring time. The model correctly reproduces the summertime direction of the wind stress in the eastern Pacific. The model also exhibits realistic seasonality in the interannual variability of ENSO measures by the interannual variance of the Niño-3.4 index (not shown here).

The simulated interannual variance peaks during late autumn and winter, similar to observations.

Another very important phase lock feature is exhibited in the annual cycle of the correlation between Niño-3 SST anomalies and the Indian Ocean dipole (IOD). Figure 7 shows the correlation between different indices associated with IOD and the Niño-3.4 index. The IOD index is based on the difference in SST between the west (10°S – 10°N , 50° – 70°E) and southeast (5°S – 0° , 90° – 110°E) tropical Indian Ocean. The ENSO signal propagates (via the atmosphere) into the Indian Ocean and results in the substantial correlation between Niño-3.4 and the western node of the Indian dipole. The amplitudes and phases of the correlations between the IOD and Niño-3.4 are very similar to observations (e.g., see Fig. 19 in Johns et al. 2006). In contrast to some other coupled models (e.g., HADGEM1), the ECPM produces a more realistic phase lock between the IOD and Niño-3.4.

b. Interannual variability

As was noted in a vast number of studies (e.g., Delworth et al. 2006) the standard deviation of the annual-mean SST can be considered to be one of the robust measures of the model internal variability. Figure 8 shows the ECPM and NCEP OI SST interannual standard deviation. The model SSTs include 56 yr of simulations. The NCEP OI SSTs were taken for the period of 1950–2005. The linear trend was removed from both datasets. The model variability pattern is similar to the observation in the eastern and central tropical Pacific, as well as over the midlatitude Pacific. As in the case with some other coupled models (e.g., GFDL CM2.0 and CM2.1; Delworth et al. 2006), ECPM exaggerates SST variability, especially in the Tropics and over the Oyashio Extension region.

To further document the interannual variability in the model, a spectral analysis of the 56 yr of the simulated wintertime SST anomalies averaged over Niño-3.4 region (5°N – 5°S , 170° – 120°W ; Fig. 9) was compared with the spectra of the wintertime NCEP OI SST (Reynolds and Smith 1994) from 1950 to 2005. It should be noted that the spectral analysis was performed on a wintertime data because of the pronounced phase lock discussed in the previous section. The ECPM spectra exhibits statistically significant maxima peaks in the 2–6-yr period interval, which are comparable to analogous peaks obtained from observed NCEP OI SSTs. These peaks correspond to quasi-periodic ENSO events.

Figure 10 shows wintertime SSTAs averaged over the Niño-3.4 region. ECPM exhibits a slightly stronger amplitude of variability. This difference is further con-

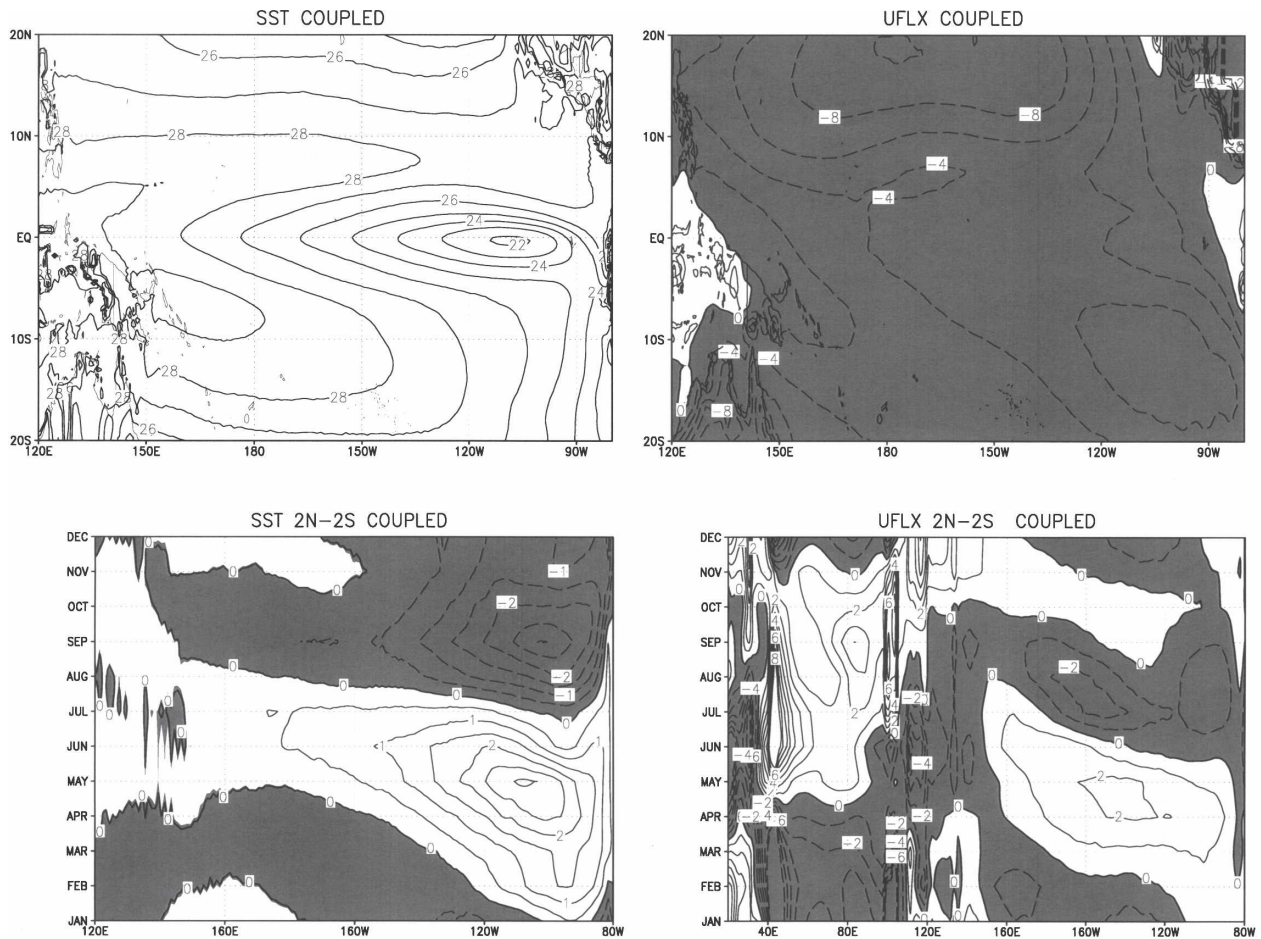


FIG. 6. (top left) ECPM annual mean SSTs in the Tropics. The contour interval is 1 K. (top right) ECPM annual mean zonal wind stress ($\times 10^2$) in the Tropics. The contour interval is 2 N m^{-2} . (bottom left) Annual cycle along the equator (2°N – 2°S) of the deviations from the annual mean ECPM SSTs. The contour interval is 0.5 K. (bottom right) The deviations from the annual mean ECPM zonal wind stress ($\times 10^2$). The contour interval 1 N m^{-2} . Negative values are shaded.

firmed by a comparison between the simulated (bottom-left panel, Fig. 10) and observed (bottom-right panel, Fig. 10) frequency distributions of the Niño-3.4 SST anomalies. The probability of the simulated El Niño events is slightly greater than the probability of La Niña events, the amplitude of the warm extreme events in the model is also slightly larger than of the cold events. This is opposite to the simulations by HadGEM1 (Johns et al. 2006) that produces weaker-than-observed variability for the positive-phase SST anomalies.

c. ENSO evolution

The evolution of ENSO can be expressed by constructing the maps of the equatorial SST, wind stress, upper-ocean current, and temperature lag regressed onto the Niño-3 index (SST anomalies averaged over 5°S – 5°N and 150° – 90°W). Figure 11 shows the ECPM lag regressions onto the Niño-3 index normalized by

one standard deviation. Positive time corresponds to Niño-3 leading the variable. All the fields were averaged over 2°N – 2°S . SST anomalies are zonally uniform and nearly steady from 80°W to 130°E . The SST anomalies peak approximately 12 months after they start to develop in the western Pacific. The SST anomalies over the westernmost Pacific are negative at the time of the nearly basinwide peak. These cold anomalies propagate eastward reaching the equatorial part of the American coast in about 12 months. This behavior is very similar to the observed anomalies of the Extended Reconstructed SST, version 2 (ER.v2), presented by Wittenberg et al. (2006, their Fig. 23).

The equatorial zonal wind stress anomalies propagate eastward. However, in comparison to the ERA-40 zonal wind stress anomalies (see Wittenberg et al. 2006), there is a steady westerly anomaly pattern over the western part of the equatorial Pacific, up to around

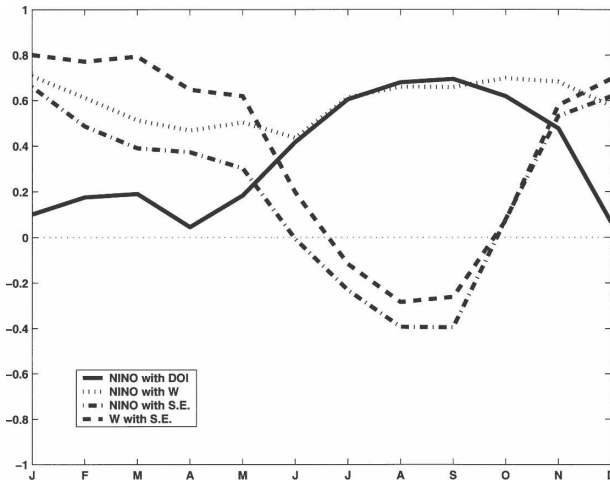


FIG. 7. Annual cycle of the correlation between 1) the IOD index [based on the difference in SST between the west (10°S–10°N, 50°–70°E) and southeast (5°S–0°, 90°–110°E) tropical Indian Ocean] and Niño-3.4 index (solid line); 2) the western node of the IOD and the Niño-3.4 index (dotted line); 3) the southeast node of the IOD and the Niño-3.4 index (dashed-dotted line); and 4) the west and southeast nodes of IOD (dashed line).

130°E. This steady pattern is produced by the GFDL CM2.0 and CM2.1 as well and is due to the lack of stochastic noise in the atmospheric forcing (B. Kirtman 2006, personal communications). As in the observations, the peak in the wind stress anomalies over the central Pacific is preceded by westerlies over the western Pacific nearly 12 months before the peak. The peak occurs over the central Pacific a couple months before the peak in SSTAs. In the ECPM, the easterlies reappear in the west and central Pacific in 9 months, which is different from the observations that show eastward propagation of easterlies. It should be noted, that the

GFDL CM2.0 and CM2.1 do not correctly reproduce this propagation as well.

As in the GFDL Applied Research Center ocean analysis (Wittenberg at al. 2006), ECPM reproduces the eastward propagation of the upper-ocean heat content that peaks at the time of the SSTAs peak. However, there is a difference in the propagation of the cold upper-ocean temperature anomalies from the western Pacific. As is the case with the wind stress anomalies, the cold ocean anomalies reappear in the central and eastern Pacific, instead of propagating eastward.

The upper-ocean eastward zonal currents peak in the easternmost Pacific 3–12 months before the SSTAs peak. The western currents then start to develop around the ENSO peak. The pattern of westward currents encompasses nearly the whole basin and is centered over the central Pacific. These currents reach maxima 6–9 months after the SSTAs peak. This development is similar to the evolution of GFDL CM2.0/CM2.1 currents (e.g., Wittenberg et al. 2006). Because the zonal current advection of the SST gradient is crucial in transition from El to La Niño, the qualitative similarity between ECPM simulations of the ocean currents and observations is crucial for correct ENSO simulations.

To summarize, the ECPM simulation of the ENSO mechanism is qualitatively similar to the observations. The differences are not worse than the ones produced by other (e.g., GFDL CM2.0/CM2.1) coupled models. We are planning to eventually perform more detailed studies on the cause of these discrepancies.

d. ENSO teleconnection patterns

As was noted in the variety of studies, the climate system has a global response to the ENSO forcing.

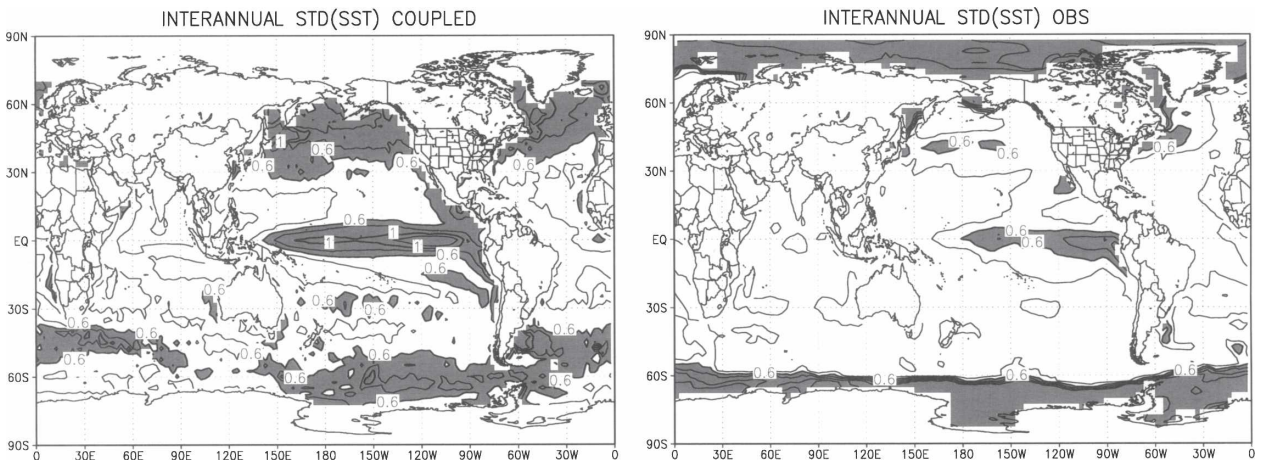


FIG. 8. Standard deviation of the annual-mean SST (K) from (left) ECPM 56 yr of simulations and (right) NCEP OI SST for the period of 1950–2005. The contour interval is 0.2 K.

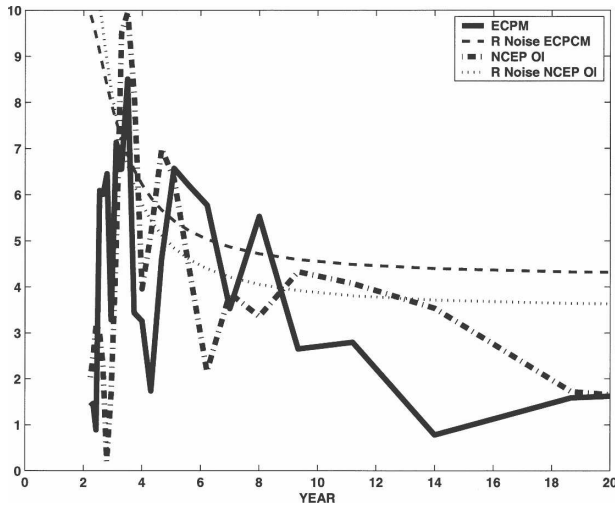


FIG. 9. Spectral analysis of the wintertime Niño-3.4 (5°N–5°S, 170°–120°W) ECPCM SSTAs obtained from the 56-yr integration (solid line) and NCEP–DOE OI SSTAs for 1950–2005 period (dash-dotted line). The corresponding red noise spectra (dashed line for ECPCM and dotted line for OI SST) indicate the significance of the power peaks.

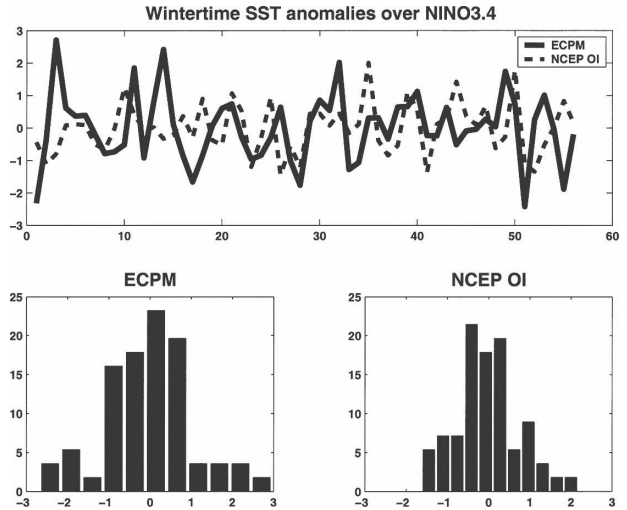


FIG. 10. (top) Wintertime SSTAs averaged over the Niño-3.4 region simulated by ECPCM (solid line) and NCEP OI SST (dashed line). (bottom) The frequency distribution of the Niño-3.4 SSTAs in (left) ECPCM and (right) NCEP OI SST data. A total of 56 yr of ECPCM simulations were used. NCEP OI SST data are for the 1950–2005 time period.

These teleconnection patterns have been extensively studied and documented (e.g., Wallace and Gutzler 1981; Sardeshmukh et al. 2000). The spatial pattern of the SST response is shown in Fig. 12. The correlation map between the Niño-3.4 index and SSTAs over the Pacific produced by the ECPCM is qualitatively similar to the observed NCEP OI SST map. The meridional structure and strength simulated by the model over the Pacific are in good agreement with observations. The weaker signals over the Indian and Atlantic Oceans are also similar to the observations.

We also studied the skill of ECPCM to produce an ENSO-related remote atmospheric response by regressing 500-hPa height (Z500) anomalies onto the Niño-3.4 index. The response in Z500 to one standard deviation of the ENSO signal in the ECPCM (not shown here) over midlatitudes bears similarities with the analogous response in R-2 data, indicating that our coupled model reproduces, reasonably well, the atmospheric Tropics–midlatitude bridge.

Another test of the skill of a coupled model is its ability to correctly simulate the relationship between SST and heat flux anomalies, especially over the North Pacific, and in the tropical monsoon regions, where the atmosphere significantly alters SST variability. We investigated the local correlation between SST anomalies and latent heat fluxes. Figure 13 compares the correlation between SST and latent heat anomalies for ECPCM (top panel) and for the AMIP run with the same atmospheric component. This figure can be compared with

the Center for Ocean–Land–Atmosphere (COLA) coupled and stand-alone models (Fig. 7 from Wu et al. 2006). As opposed to the stand-alone atmospheric integration, both the ECPCM and coupled COLA model produce negative correlations in the tropical Pacific and equatorial Indian Oceans, indicating that SST anomalies in these regions are forced by the atmosphere. Although the correlations over the western part of the Pacific warm pool in the coupled model are negative, the region of positive correlations still extends too much to the west in comparison to observations [see map of pointwise correlations derived from the Goddard Satellite-based Surface Turbulent Fluxes, version 2, latent heat flux anomalies and observed SST anomalies shown in Fig. 6 from Wu et al. (2006)]. Similar errors occur in the UCLA coupled atmosphere–ocean general circulation model (Yu and Mechoso 1999). However, in comparison to the uncoupled run, the introduction of the coupling improves the skill of the heat flux simulation over the equatorial Indian Ocean and western tropical Pacific, two regions that are crucial for monsoon development (Wu et al. 2006).

The skill of ECPCM in producing the monsoon–ENSO relationship is shown in Fig. 14. The figure shows the correlation between June–September precipitation averaged over India (5°–25°N, 60°–100°E) and SSTAs during the next winter season (DJF). As was shown in Kirtman and Shukla (2002), the uncoupled AGCMs do not correctly simulate this relationship. Figure 14 shows lots of similarities between simulated by ECPCM (top

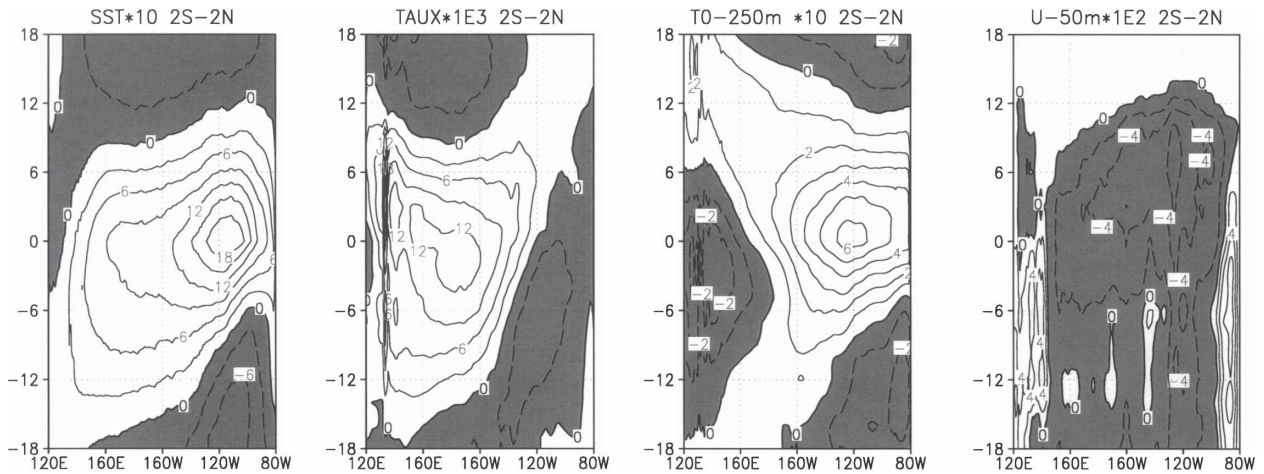


FIG. 11. ECPM lag regression maps obtained by regressing onto the normalized Niño-3 index. (from left to right) SST (K K^{-1}), zonal wind stress anomalies ($\text{N m}^{-2} \text{K}^{-1}$), upper-ocean temperature averaged over the upper 250 m (K K^{-1}), upper-ocean zonal current averaged over the upper 50 m ($\text{m s}^{-1} \text{K}^{-1}$). All fields are averaged over 2°S – 2°N . The time goes from -18 months to $+18$ months. Positive time means that the Niño-3 index is leading. Negative values are shaded.

panel) and observed (bottom panel) correlation maps. The observed correlation map was derived from the Climate Anomaly Monitoring System (CAMS) precipitation data and NCEP OI SSTs. The coupled model correctly captures broad tropical Pacific and Indian Ocean negative correlation patterns. This result is comparable with the correlation pattern produced by the COLA ACGCM (Kirtman and Shukla 2002). Therefore, it is safe to say that our coupled model has good skill in simulating the Indian monsoon–ENSO relationship.

Because of the lack of disk storage, we did not save daily data for this initial run; thus, we are not able to

analyze the skill of simulating higher-frequency MJO and storm tracks. However, in the future, we do plan to analyze higher-frequency processes in the coupled model.

5. Skill of the retrospective forecast

We performed ECPM retrospective forecasts for different months. The initial oceanic conditions were obtained directly from the JPL 1994–2005 ocean analysis. Because we use the same ocean model configuration as the JPL analysis, our model forecast starts smoothly from the ocean analysis, without any noticeable initial

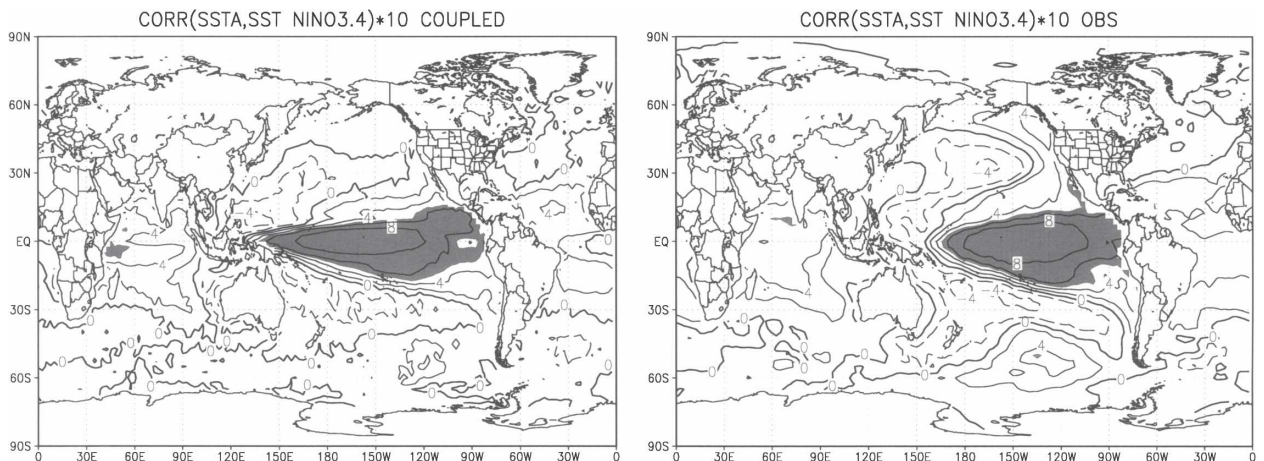


FIG. 12. Correlation ($\times 10$) between Niño-3.4 SST anomalies and global SST anomalies: (left) 56 yr of ECPM integration; (right) NCEP OI SST anomalies during 1950–2005. The contour interval is 2. Shading indicates correlations greater than 95% significance level.

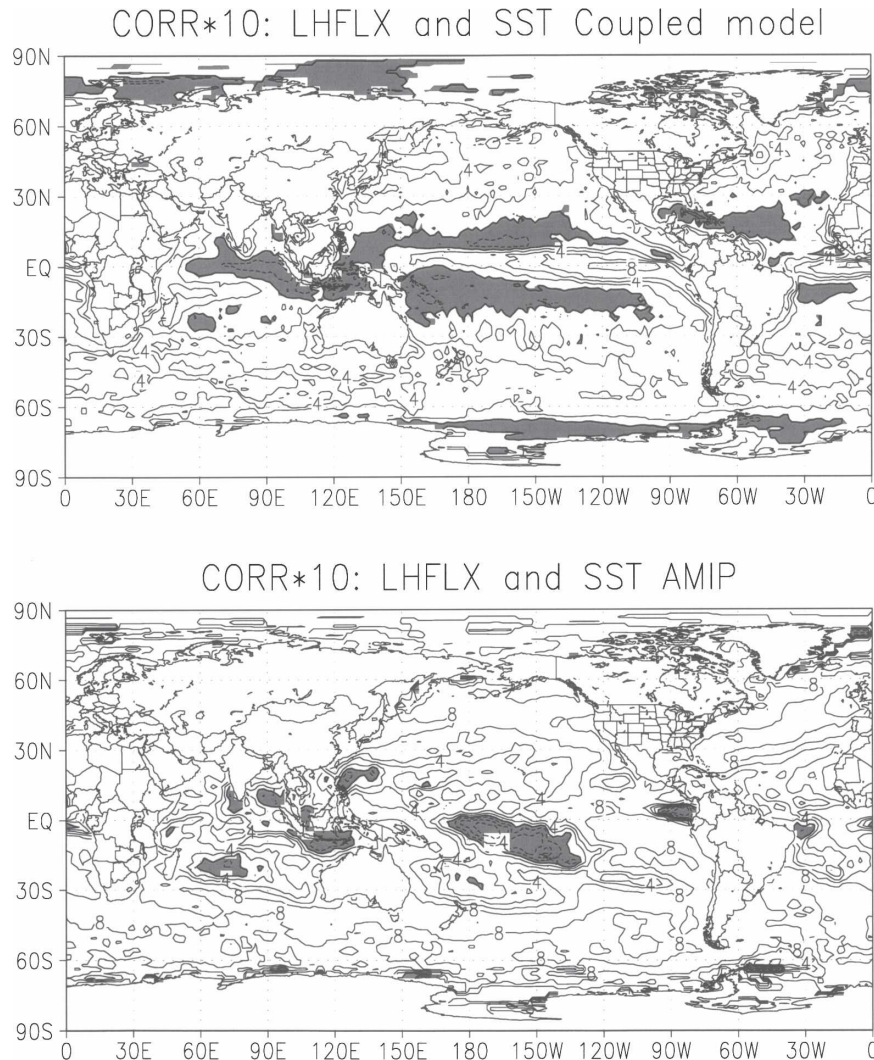


FIG. 13. Correlation ($\times 10$) between SST and latent heat anomalies from (top) ECPM and (bottom) AMIP GSM integration data. The contour interval is 2. Shading indicates correlations greater than 95% significance level.

shocks. We have now performed 1-yr predictions starting at the beginning of each month from 1994 to the present. The climatology derived from these retrospective forecasts is used to obtain the anomalies for the real-time forecast. The skill of the Niño-3.4 predictions, measured by the correlation between the simulated SST Niño-3.4 anomalies and the observation (Fig. 15), demonstrates that the skill of the forecasts initiated in winter usually drops by the fourth month (spring barrier), but then picks up again and stays high for up to 12 months after the coupled model dynamics starts to influence the predictability. The skill of the forecasts started in summer is very high for up to 9 months of lead time. The correlation values smaller than 0.52 (95% confidence level for 12 degrees of freedom) are

masked. The ECPM skill seasonal dependency is similar to the one obtained from the NCEP CFS (Saha et al. 2006). Analogous skill (not shown here) for the North Pacific–North American 500-hPa height also indicates a drop in prediction skill by the sixth month of integration.

Based on this initial ensemble of predictions, we have now started to produce near-real-time experimental seasonal forecasts (see online at <http://ecpc.ucsd.edu/COUPLED/CM/coupled.html>). Figure 16 demonstrates the relationship between the ECPM SST anomalies forecast and predictions by the dynamical models used for IRI SST anomalies forecasts in the Niño-3.4 region for 2004–05 forecasts started at the beginning of each month from May to December. The

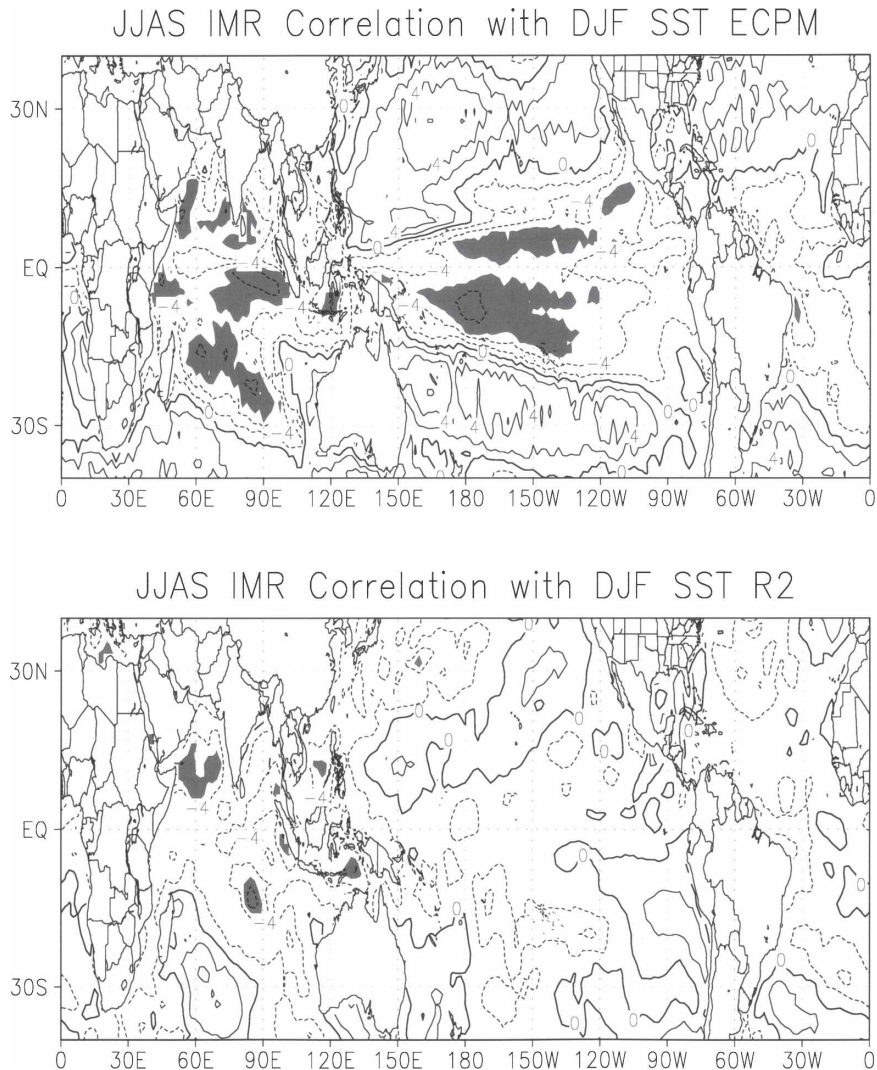


FIG. 14. Correlation ($\times 10$) between Indian summer (June–September) monsoon rainfall and the subsequent winter season DJF SSTAs: (top) ECPM; (bottom) CAMS precipitation and NCEP OI SSTs contour interval 2. Shading indicates correlations greater than 95% significance level.

scatterplot includes the forecasts from the following models: NASA's Seasonal-to-Interannual Prediction Project (NSIPP) model, the NCEP CFS, Japan Meteorological Agency's model, Scripps Institution's hybrid coupled ocean–atmosphere model, the Lamont-Doherty model, the Predictive Ocean Atmosphere Model for Australia (POAMA), the ECMWF model, the Met Office model, the Seoul National University (Korea) model, Zhang's intermediate coupled model, the ECHAM/MOM, and the COLA Anomaly model. (The data were obtained from <http://iri.columbia.edu/climate/ENSO/currentinfo/archive/index.html>.) The diagonal line indicates a perfect prediction. The closer the point to the line, the better the prediction. The IRI

models exhibit large scatter in the fourth quadrant, meaning that there is a large error in negative Niño-3.4 SST anomalies prediction. The ECPM has smaller errors in the fourth quadrant, as well as smaller scatter around the red line. Again, it should be noted that our forecast skill evaluation is preliminary because it is based on a smaller number of realizations than larger ensemble predictions from the other models.

The skill of 4–6-months lead prediction of DJF (from initial conditions centered at 1 August) near-surface variables (precipitation and 2-m temperature), measured by correlation between observed and predicted anomalies, is shown in Fig. 17. The correlation coefficients greater than the 95% statistical significance level

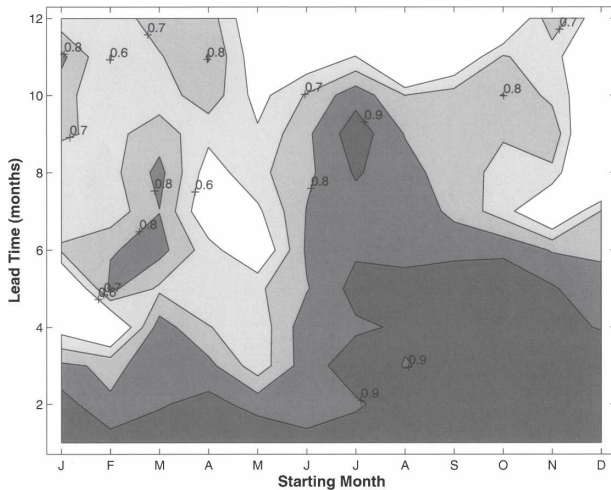


FIG. 15. The skill of the Niño-3.4 predictions measured by the correlation between ECPM and NCEP/DOE OI Niño-3.4 SST anomalies. Correlation coefficients that are less than 95% significance level cutoff are masked.

cutoff are shaded. ECPM has some skill in predicting 2-m temperature (T2m) over the northwestern parts of the United States and part of the west coast of Canada and Alaska. The model has a good skill in predicting precipitation over the northeastern part of the United

States and Alaska. For these regions, the model skill is similar to the skill of the FSU climate model coupled to the NCAR Community Land Model, version 2, as discussed in Shin et al. (2005).

Figure 18 shows the skill of the model in 4–6-months lead prediction of the oceanic 400-m heat content and temperature along the equator. The top panel shows the correlation between DJF 1994–2005 anomalies predicted from the ECPM integrations started at the beginning of August and the corresponding anomalies from the JPL analysis of the DJF 400-m heat content. Though the correlations are very high over the tropical Pacific Ocean, the ECPM skill is poor over the tropical Indian Ocean.

The corresponding skill in predicting equatorial temperature in the Pacific Ocean is shown in the bottom panel in Fig. 18. The depth–longitude cross section of the correlation between ECPM and the JPL equatorial DJF temperature anomalies exhibits high skill in predicting oceanic temperatures over this region.

6. Summary and further work

We summarize the description and skill of some prominent coupled models currently being used for seasonal climate predictions in Table 1. The skill is mea-

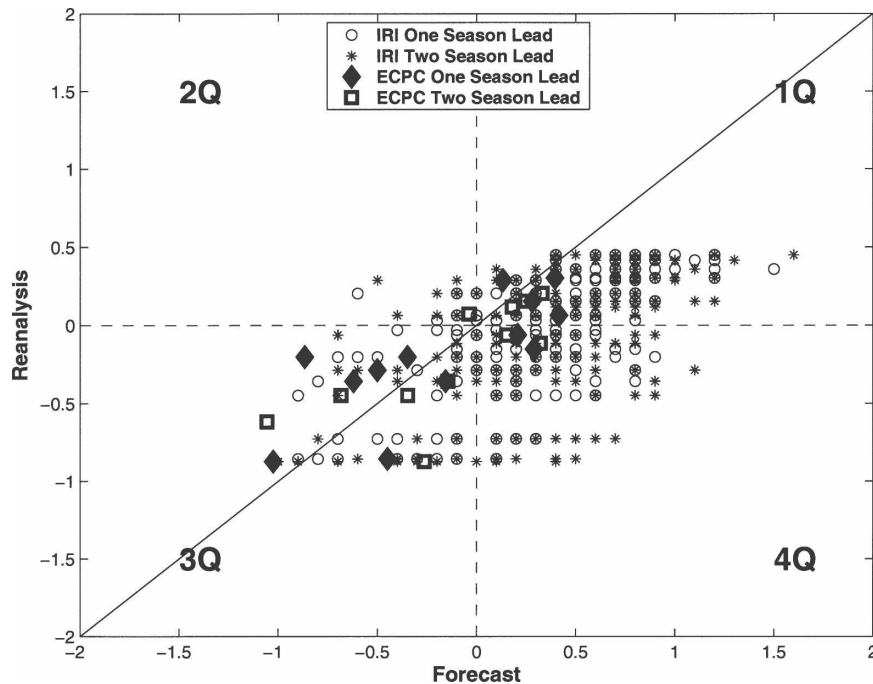


FIG. 16. Scatterplot of Niño-3.4 SST anomalies predictions (2004–05) started at the beginning of each month from May to December vs NCEP/DOE OI SSTAs. The diagonal line indicates perfect prediction, the closer the point to the line, the better the prediction. The IRI models exhibit large scatter in the fourth quadrant, meaning that there is a large error for negative Niño-3.4 SST anomaly predictions. ECPM has smaller errors in the fourth quadrant, as well as smaller scatter about the red line.

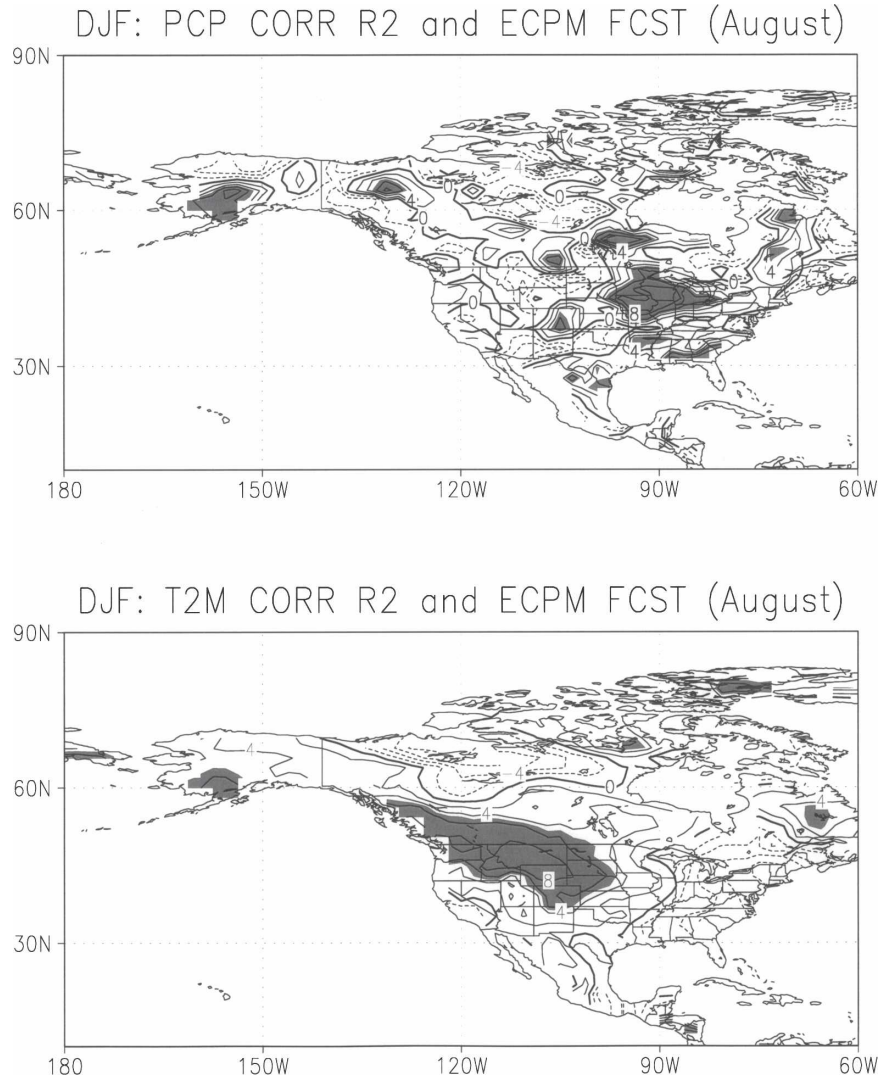


FIG. 17. Skill of the 4–6-months lead DJF prediction of near-surface variables: precipitation and T2m from forecasts started at the beginning of August for the 1994–2005 time period. Correlations coefficients that are greater than 95% significance level cutoff are shaded.

sured by correlation coefficients (for the period of 1994–2005) between predicted wintertime DJF anomalies (4–6-months lead forecasts initialized in August) and observed DJF anomalies. The correlation coefficients were averaged over the western United States for 2-m temperature and the southeastern United States for precipitation (regions with the correlations greater than 0.5 on the maps in Fig. 17). Data for the Development of a European Multimodel Ensemble System for Seasonal-to-Interannual Prediction (DEMETER) models was obtained from the DEMETER Web site. Only one ensemble member was used for these calculations. Compared with other models, ECPM exhibits relatively good skill in predicting precipitation and T2m

over the selected U.S. areas. Again, the main drawback is that we have not yet had the resources to perform many additional ensemble forecasts and because of the availability of JPL assimilation ocean analysis, the forecasts are based only on the 1994–2005 period. However, these preliminary results are promising and provide an indication of the potential of the ECPM. In the future we will compare ECPM with the 11 coupled models that were assessed by Lawrence Livermore National Laboratory’s Program for Climate Model Diagnosis and Intercomparison (Philips et al. 2006).

The main reasons why ECPM should now be included into the mix of similar coupled models including the one developed at NCEP are as follows:

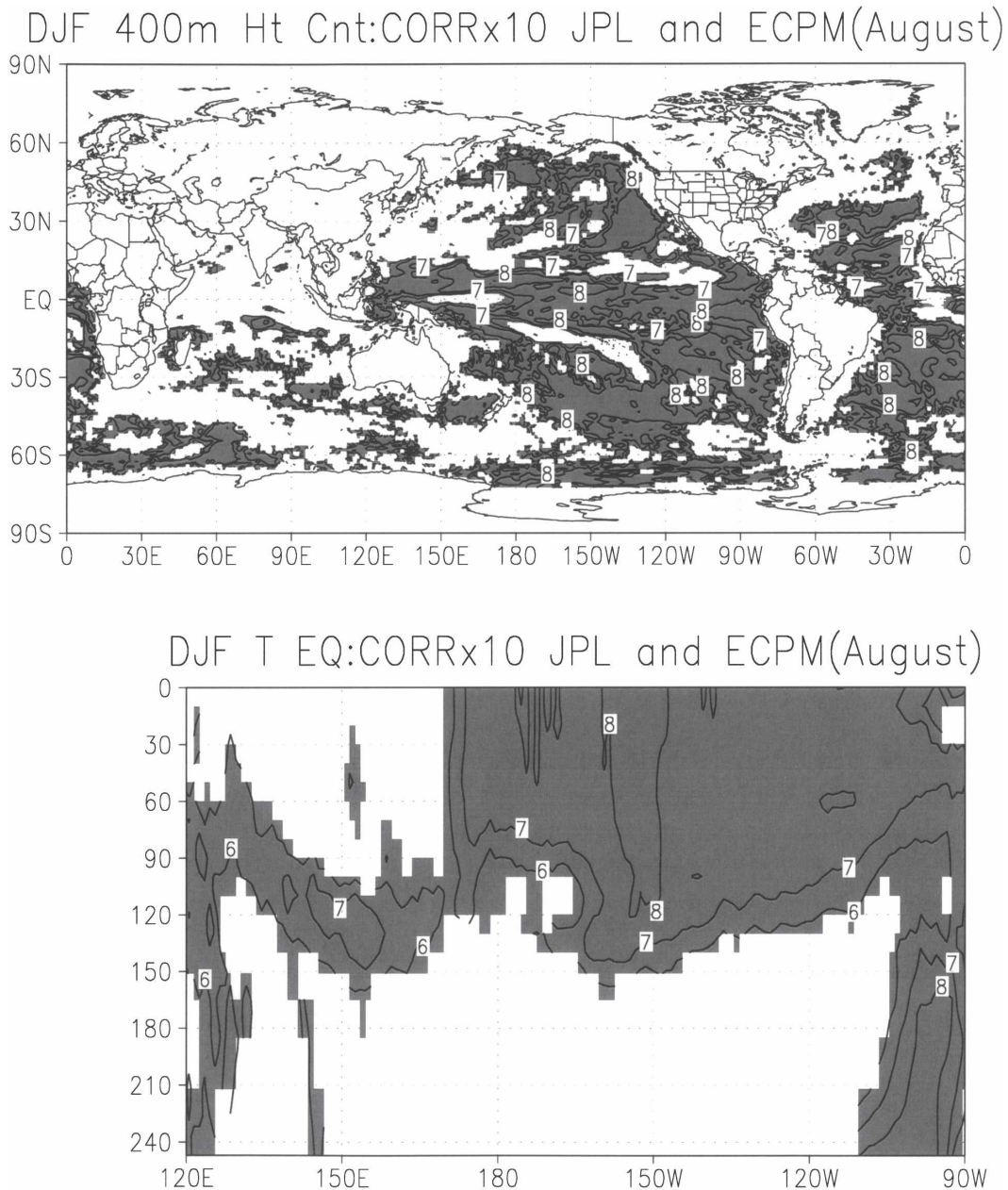


FIG. 18. (top) The correlation ($\times 10$) between DJF 1994–2005 anomalies predicted from the ECPM integrations started in August and the corresponding anomalies from the JPL analysis of the DJF 400-m heat content. The contour interval is 1. (bottom) Same as (top), but for the depth–longitude cross section of the correlation between ECPM and JPL equatorial DJF temperature anomalies. The contour interval is 1. Correlation coefficients that are less than the 95% significance level cutoff are masked.

- Both ECPC atmospheric and ocean models are very nearly identical to the ones used for data assimilation, thus, initial conditions for both the atmosphere and ocean are consistent and initial spinup is small. This is also true for NCEP CFS, NASA NSIPP, COLA, and other systems that perform ocean data assimilation.
- The assimilation version of the JPL MIT OM is used

routinely to produce a 4D ocean state assimilation. The consortium for Estimating the Circulation and Climate of the Ocean has already demonstrated the feasibility and utility of providing global, sustained, dynamically sensible estimates for the full three-dimensional, time-varying oceanic state and associated surface forcing fields required to bring the

TABLE 1. Skill (measured by correlation) of coupled model predictions for the U.S. regions. Forecast skill of ECPM and DEMETER models in predicting precipitation and T2m over the United States. Skill is measured by correlation coefficients (for the period of 1994–2005) between predicted wintertime DJF anomalies (4–6 months of lead forecasts initialized in August) and observed DJF anomalies. The correlation coefficients were averaged over the western United States for 2-m temperature and the southeastern United States for precipitation (regions with the correlations greater than 0.5 on the maps in Fig. 17). Data for the DEMETER models were obtained from the DEMETER Web site. Only one ensemble member was used for these calculations. ARPEGE: Action de Recherche Petite Echelle Grande Echelle; IFS: Integrated Forecast System; HOPE-E: Hamburg Ocean Primitive Equation; OPA: Océan Parallélisé; HadCM3: Third Hadley Centre Coupled Ocean–Atmosphere General Circulation Model; HadAM3: Third Hadley Centre Atmosphere Model.

Model	Ocean	Atmosphere	4–6-months lead skill precipitation	4–6-months lead skill: T2m
CERFACS	OPA8.2 2 × 2, L31	ARPEGE T63, L31	0.5	0.7
ECMWF	HOPE-E; 1.4 × 0.3–1.4, L29	IFS, T95, L40	0.5	0.7
LODYC	OPA8.2 2 × 2, L31	IFS, T95, L40	0.7	0.5
Met Office	OGCM based on HadCM3; 1.25 × 0.3–1.25, L40	HadAM3, 2.5 × 3.75, L19	0.7	0.5
MPI	MPI, 1.5 × 1.5 L40	ECHAM5, T63L31	0.6	0.4
ECPM	MIT 1 × 1/3–1, L46	GSM T62, L28	0.6	0.7

model into consistency with ocean observations. The use of the 4D variational ocean assimilation system to minimize the initial drift of the ocean model may be an improvement upon the older GFDL assimilation system in use at NCEP.

- The ocean model component is different from that in other coupled models. Different ocean models and assimilation systems are needed to span the natural uncertainty associated with ocean initial conditions and forecasts.
- These global coupled model simulations and forecasts are beginning to be used as boundary conditions for regional coupled model simulations and forecasts. In particular, we are beginning to develop a corresponding regional coupled atmosphere–ocean model that can be used in coastal regions (Seo et al. 2007).

To develop the coupled ocean–atmosphere–land model for long lead climate prediction (multiseasons), we are now planning to further assess the skill of the coupled model retrospective forecasts and compare this skill with the two-tiered prediction model. As was shown, the skill of the forecasts depends on the start date and targeted season, and thus should be similar to the skill found in other coupled models. To get more statistically robust results, especially for individual predictions, we intend to perform 10-member ensemble predictions for each month of the recent 14-yr period (the JPL ocean state analysis is updated monthly and is available from 1993 to the present). A single initial condition will be used for the ocean initial condition because only single oceanic initial conditions are available each month. However, the multiple initial conditions for the atmosphere ensemble will be extracted from R-2 from every 12-h initial state nearest to the beginning of each month.

We will also study the idealized predictability of the coupled model. For this purpose, we intend to perform a long (100 yr) 10-member ensemble coupled model simulation without any flux correction. We will use this coupled long simulation as a proxy for an observed state, and perform two-tier and additional coupled runs with perturbed initial conditions of the ocean and atmosphere. We will then compare the statistics from these runs with the original long coupled integration as well as with the actual forecast experiments. This effort could provide a possible upper boundary to coupled predictability, which may then be useful for helping us to better understand the ultimate capability of our coupled model.

Acknowledgments. This research was funded by a cooperative agreement from NOAA-NA17RJ1231. The views expressed herein are those of the authors and do not necessarily reflect the views of NOAA. We gratefully acknowledge JPL and NCEP for providing the initial analyses being used for our experimental long-range prediction effort. Special thanks go to Drs. D. Stammer and I. Fukumori and their groups for providing assistance with the MIT ocean model. The computations were performed on PC cluster at SIO, and at NCAR on CSL machines.

REFERENCES

- Alpert, J. C., M. Kanamitsu, P. M. Caplan, J. G. Sela, G. H. White, and E. Kalnay, 1988: Mountain induced gravity wave drag parameterization in the NMC medium-range model. Preprints, *Eighth Conf. on Numerical Weather Prediction*, Baltimore, MD, Amer. Meteor. Soc., 726–733.
- Asselin, R., 1972: Frequency filter for time integrations. *Mon. Wea. Rev.*, **100**, 487–490.
- Baldwin, M. P., and T. J. Dunkerton, 1999: Propagation of the

- Arctic oscillation from the stratosphere to the troposphere. *J. Geophys. Res.*, **104**, 30 937–30 946.
- Bourke, W., 1974: A multi-level spectral model. I. Formulation and hemispheric integrations. *Mon. Wea. Rev.*, **102**, 687–701.
- Carton, J. A., G. Chepurin, X. Cao, and B. Giese, 2000: A simple ocean data assimilation analysis of the global upper ocean, 1950–95. Part I: Methodology. *J. Phys. Oceanogr.*, **30**, 294–309.
- Cazes-Boezio, G. D., D. Menemenlis, and C. R. Mechoso, 2008: Impact of ECCO ocean-state estimates on the initialization of seasonal climate forecasts. *J. Climate*, in press.
- Chou, M.-D., and M. J. Suarez, 1994: An efficient thermal infrared radiation parameterization for use in general circulation models. NASA Tech. Rep. TM-1994-104606, Vol. 3, 85 pp.
- , and K.-T. Lee, 1996: Parameterizations for the absorption of solar radiation by water vapor and ozone. *J. Atmos. Sci.*, **53**, 1203–1208.
- Delworth, T. L., and Coauthors, 2006: GFDL's CM2 global coupled climate models. Part I: Formulation and simulation characteristics. *J. Climate*, **19**, 643–674.
- Derber, J., and A. Rosati, 1989: A global oceanic data assimilation system. *J. Phys. Oceanogr.*, **19**, 1333–1347.
- Dickey, J. O., S. L. Marcus, O. de Viron, and I. Fukumori, 2002: Recent Earth oblateness variations: Unraveling climate and postglacial rebound effects. *Science*, **298**, 1975–1977.
- Fukumori, I., 2002: A partitioned Kalman filter and smoother. *Mon. Wea. Rev.*, **130**, 1370–1383.
- GFDL Global Atmospheric Model Development Team, 2004: The new GFDL global atmosphere and land model AM2–LM2: Evaluation with prescribed SST simulations. *J. Climate*, **17**, 4641–4673.
- Gordon, C., C. Cooper, C. A. Senior, H. Banks, J. M. Gregory, T. C. Johns, J. F. B. Mitchell, and R. A. Wood, 2000: The simulation of SST, sea ice extents and ocean heat transports in a version of the Hadley Centre coupled model without flux adjustments. *Climate Dyn.*, **16**, 147–168.
- Hong, S.-Y., and H.-L. Pan, 1996: Nonlocal boundary layer vertical diffusion in a medium-range forecast model. *Mon. Wea. Rev.*, **124**, 2322–2339.
- Ji, M., A. Leetmaa, and J. Derber, 1995: An ocean analysis system for seasonal to interannual climate studies. *Mon. Wea. Rev.*, **123**, 460–481.
- , D. W. Behringer, and A. Leetmaa, 1998: An improved coupled model for ENSO prediction and implications for ocean initialization. Part II: The coupled model. *Mon. Wea. Rev.*, **126**, 1022–1034.
- Johns, T. C., and Coauthors, 2006: The new Hadley Centre climate model (HadGEM1): Evaluation of coupled simulations. *J. Climate*, **19**, 1327–1353.
- Juang, H.-M. H., 2004: A reduced spectral transform for the NCEP seasonal forecast global spectral atmospheric model. *Mon. Wea. Rev.*, **132**, 1019–1035.
- Jungclaus, J. H., and Coauthors, 2006: Ocean circulation and tropical variability in the coupled model ECHAM5/MPI-OM. *J. Climate*, **19**, 3952–3972.
- Kalnay, E., and M. Kanamitsu, 1988: Time schemes for strongly nonlinear damping equations. *Mon. Wea. Rev.*, **116**, 1945–1958.
- Kanamitsu, M., and Coauthors, 1991: Recent changes implemented into the global forecast system at NMC. *Wea. Forecasting*, **6**, 425–435.
- , and Coauthors, 2002a: NCEP dynamical seasonal forecast system 2000. *Bull. Amer. Meteor. Soc.*, **83**, 1019–1037.
- , W. Ebisuzaki, J. Woollen, S.-K. Yang, J. J. Hnilo, M. Fiorino, and G. L. Potter, 2002b: NCEP–DOE AMIP-II Reanalysis (R-2). *Bull. Amer. Meteor. Soc.*, **83**, 1631–1643.
- , C.-H. Lu, J. Schemm, and W. Ebisuzaki, 2003: The predictability of soil moisture and near-surface temperature in hindcasts of NCEP seasonal forecast model. *J. Climate*, **16**, 510–521.
- Kirtman, B., and J. Shukla, 2002: Interactive coupled ensemble: A new coupling strategy for CGCMs. *Geophys. Res. Lett.*, **29**, 1367, doi:10.1029/2002GL014834.
- Large, W. G., J. C. McWilliams, and S. C. Doney, 1994: Oceanic vertical mixing: A review and a model with nonlocal boundary layer parameterization. *Rev. Geophys.*, **32**, 363–403.
- Leith, C. E., 1971: Atmospheric predictability and two-dimensional turbulence. *J. Atmos. Sci.*, **28**, 145–161.
- Li, T., and S. G. H. Philander, 1996: On the annual cycle of the eastern equatorial Pacific. *J. Climate*, **9**, 2986–2998.
- Marshall, J., A. Adcroft, C. Hill, L. Perelman, and C. Heisey, 1997a: A finite volume, incompressible Navier-Stokes model for studies of the ocean on parallel computers. *J. Geophys. Res.*, **102**, 5753–5766.
- , C. Hill, L. Perelman, and A. Adcroft, 1997b: Hydrostatic, quasi-hydrostatic and nonhydrostatic ocean modeling. *J. Geophys. Res.*, **102**, 5733–5752.
- Martin, G. M., M. A. Ringer, V. D. Pope, A. Jones, C. Dearden, and T. J. Hinton, 2006: The physical properties of the atmosphere in the new Hadley Centre Global Environmental Model (HadGEM1). Part I: Model description and global climatology. *J. Climate*, **19**, 1274–1301.
- McPhaden, M. J., 2004: Evolution of the 2002/03 El Niño. *Bull. Amer. Meteor. Soc.*, **85**, 677–695.
- Megann, A. P., A. L. New, and B. Sinha, 2005: Comparisons between the CHIME coupled climate model and HadCM3. *COAPEC Newsletter*, No. 5, NERC Southampton Oceanography Centre, Southampton, United Kingdom, 7–8.
- Menemenlis, D., I. Fukumori, and T. Lee, 2005: Using Green's functions to calibrate an ocean general circulation model. *Mon. Wea. Rev.*, **133**, 1224–1240.
- Moore, A. M., and R. Kleeman, 1996: The dynamics of error growth and predictability in a coupled model of ENSO. *Quart. J. Roy. Meteor. Soc.*, **122**, 1405–1446.
- Moorthi, S., and M. J. Suarez, 1992: Relaxed Arakawa-Schubert: A parameterization of moist convection for general circulation models. *Mon. Wea. Rev.*, **120**, 978–1002.
- Pan, H.-L., and L. Mahrt, 1987: Interaction between soil hydrology and boundary layer development. *Bound.-Layer Meteor.*, **38**, 185–202.
- Phillips, N. A., 1959: Numerical integration of the primitive equations on the hemisphere. *Mon. Wea. Rev.*, **87**, 333–345.
- Phillips, T. J., and Coauthors, 2006: Coupled climate model appraisal: A benchmark for future studies. *Eos, Trans. Amer. Geophys. Union*, **87**, 185.
- Reichler, T. J., and J. O. Roads, 2003: The role of boundary and initial conditions for dynamical seasonal predictability. *Nonlinear Processes Geophys.*, **10**, 211–232.
- , and —, 2004: Time-space distribution of long-range atmospheric predictability. *J. Atmos. Sci.*, **61**, 249–263.
- , and —, 2005a: Long-range predictability in the tropics. Part I: Monthly averages. *J. Climate*, **18**, 619–633.
- , and —, 2005b: Long-range predictability in the tropics. Part II: 30–60-day variability. *J. Climate*, **18**, 634–650.
- Reynolds, R. W., and T. M. Smith, 1994: Improved global sea sur-

- face temperature analyses using optimum interpolation. *J. Climate*, **7**, 929–948.
- Roads, J. O., 2004: Experimental weekly to seasonal U.S. forecasts with the regional spectral model. *Bull. Amer. Meteor. Soc.*, **85**, 1887–1902.
- , S.-C. Chen, and F. Fujioka, 2001: ECPC's weekly to seasonal global forecasts. *Bull. Amer. Meteor. Soc.*, **82**, 639–658.
- Robertson, A. W., C.-C. Ma, C. R. Mechoso, and M. Ghil, 1995: Simulation of the tropical Pacific climate with a coupled ocean-atmosphere general circulation model. Part I: The seasonal cycle. *J. Climate*, **8**, 1178–1198.
- , U. Lall, S. E. Zebiak, and L. Goddard, 2004: Improved combination of multiple atmospheric GCM ensembles for seasonal prediction. *Mon. Wea. Rev.*, **132**, 2732–2744.
- Rosati, A., K. Miyakoda, and R. Gudgel, 1997: The impact of ocean initial conditions on ENSO forecasting with a coupled model. *Mon. Wea. Rev.*, **125**, 754–772.
- Saha, S., and Coauthors, 2006: The NCEP climate forecast system. *J. Climate*, **19**, 3483–3517.
- Sardeshmukh, P. D., G. P. Compo, and C. Penland, 2000: Changes of probability associated with El Niño. *J. Climate*, **13**, 4268–4286.
- Schopf, P. S., and A. Loughe, 1995: A reduced-gravity isopycnal ocean model: Hindcasts of El Niño. *Mon. Wea. Rev.*, **123**, 2839–2863.
- Seo, H., A. J. Miller, and J. O. Roads, 2007: The Scripps Coupled Ocean–Atmosphere Regional (SCOAR) model, with applications in the eastern Pacific sector. *J. Climate*, **20**, 381–402.
- Shin, D. W., S. Cocke, T. E. LaRow, and J. J. O'Brien, 2005: Seasonal surface air temperature and precipitation in the FSU climate model coupled to the CLM2. *J. Climate*, **18**, 3217–3228.
- Slingo, J. M., 1987: The development and verification of a cloud prediction model for the ECMWF model. *Quart. J. Roy. Meteor. Soc.*, **113**, 899–927.
- Stammer, D., C. Wunsch, I. Fukumori, and J. Marshall, 2002: State estimation improves prospects for ocean research. *Eos, Trans. Amer. Geophys. Union*, **83**, 289.
- Straus, D., J. Shukla, D. Paolino, S. Schubert, M. Suarez, P. Pegion, and A. Kumar, 2003: Predictability of the seasonal mean atmospheric circulation during autumn, winter, and spring. *J. Climate*, **16**, 3629–3649.
- Tiedtke, M., 1983: The sensitivity of the time-mean large-scale flow to cumulus convection in the ECMWF model. *Proc. ECMWF Workshop on Convection in Large-Scale Models*, Reading, United Kingdom, ECMWF, 297–316.
- van Oldenborgh, G. J., M. A. Balmaseda, L. Ferranti, T. N. Stockdale, and D. L. T. Anderson, 2005: Did the ECMWF seasonal forecast model outperform statistical ENSO forecast models over the last 15 years? *J. Climate*, **18**, 3240–3249.
- Wallace, J. M., and D. Gutzler, 1981: Teleconnections in the geopotential height field during the Northern Hemisphere winter. *Mon. Wea. Rev.*, **109**, 784–812.
- Wittenberg, A. T., A. Rosati, N.-C. Lau, and J. J. Ploshay, 2006: GFDL's CM2 global coupled climate models. Part III: Tropical Pacific climate and ENSO. *J. Climate*, **19**, 698–722.
- Wu, R., B. Kirtman, and K. Pegion, 2006: Local air–sea relationship in observations and model simulations. *J. Climate*, **19**, 4914–4932.
- Yu, J.-Y., and C. R. Mechoso, 1999: A discussion on the errors in the surface heat fluxes simulated by a coupled GCM. *J. Climate*, **12**, 416–426.